Flow perturbation folding in shear zones

G. I. ALSOP[1] & R. E. HOLDSWORTH[2]

[1]*Crustal Geodynamics Group, School of Geography & Geosciences, University of St. Andrew, St. Andrews KY16 9AL, UK (e-mail: gia@st-andrews.ac.uk)*

[2]*Reactivation Research Group, Department of Earth Sciences, University of Durham, Durham DH1 3LE, UK*

Abstract: Variable patterns of displacement in shear zones may result in arcuate fold and fault traces as recognized by Mike Coward and co-workers in the early 1980s. Within such deformation zones, localized perturbations in flow may undergo acceleration (surging flow) or deceleration (slackening flow) with respect to the adjacent regions. Such flow cells may govern the orientation and geometries of folds and fabrics and thereby provide evidence of the scale and nature of deformation associated with heterogeneous flow in the high-strain zones. The length/width ratio of individual flow cells (measured in the direction of flow) may vary from <1 to >1 for situations when flow cells are, respectively, dominated by layer-parallel shear (LPS) or layer-normal shear (LNS). Folds initiating at high angles to transport are associated with LPS, whereas LNS may generate folds with slight clockwise (sinistral LNS) or anticlockwise (dextral LNS) trends relative to flow. Continued progressive deformation may subsequently modify and reduce angular relationships between folds and fabrics, but these geometric obliquities are generally preserved. Using examples from the Moine metasediments of northern Scotland, we show that folding displays predictable geometric patterns that can be related to the development of flow perturbation cells associated with Caledonian ductile thrusting under mid-crustal conditions. The differing relative timing of folds and individual ductile thrusts reflects the complexity of flow cells within ductile imbricates and additionally highlights the progressive foreland-directed propagation of ductile thrusting. These geometric relationships developed during contractional shear are compared with those generated in extensional systems, to provide an overall framework for the study of perturbation patterns. The geometric arrangement of mean fold axial planes about the flow direction results in their intersection forming parallel to the transport direction. This relationship permits transport directions to be calculated via the axial-planar intersection method (AIM), and also allows comparison with other techniques devised primarily for the study of soft-sediment deformation and palaeoslope analysis.

Shear zones may be defined as zones of relatively high strain across which significant displacement has taken place. They develop in a broad range of geological environments and therefore the study of structures associated with their development has widespread applications and implications (see Ramsay 1980; Alsop & Holdsworth 2004*a*, for a review). Folds are a particularly important field of study as they are relatively resilient to subsequent deformation and, once created, are difficult to destroy (unlike fabrics, which are more readily transposed). In addition, folds may be generated in a broad range of both materials and environments in which coherent ductile flow may operate. Folds are also readily subjected to systematic and rigorous geometric analysis and may therefore provide a unique and reliable record of deformation.

Variably oriented folds may be created by a number of mechanisms broadly categorized into two major types. Fold hinges displaying primary curvature occur where sinuous fold patterns reflect an original variation during active fold initiation and growth (e.g. Ghosh & Ramberg 1968; Dubey & Cobbold 1977). This group includes synshearing folds associated with flow perturbations (Coward & Potts 1983; Ridley 1986; Holdsworth 1990). Fold hinges displaying secondary curvature are generated when original hinge-lines are subsequently passively rotated during progressive deformation (Bryant & Reed 1969; Sanderson 1973; Escher & Watterson 1974; Rhodes & Gayer 1977; Bell 1978; Williams 1978; Ghosh & Sengupta 1984, 1987; Fossen & Rykkelid 1990; Mies 1991; Alsop 1992). Such secondary curvature may be imposed on fold hinges that may or may not display a degree of primary curvature, and may ultimately result in highly curvilinear sheath fold geometries (Carreras *et al.* 1977; Quinquis *et al.* 1978;

From: Ries, A. C., Butler, R. W. H. & Graham, R. H. (eds) 2007. *Deformation of the Continental Crust: The Legacy of Mike Coward*. Geological Society, London, Special Publications, **272**, 75–101.
0305-8719/07/$15

Minnigh 1979; Berthé & Brun 1980; Cobbold & Quiquis 1980; Skjernaa 1980, 1989; Holdsworth & Roberts 1984; Lacassin & Mattauer 1985; Goscombe 1991; Alsop 1994; Alsop & Holdsworth 1999, 2004*c*; Alsop & Holdsworth 2006).

In this study, the primary curvature of fold patterns related to surge zones within thrust belts, directly analogous to those originally studied in the early 1980s by Coward and co-workers in the Moine Thrust Zone of NW Scotland, is discussed (Coward & Kim 1981; Coward 1982, 1983, 1984; Coward & Potts 1983). The effects of differential shear on fold hinges within the more internal portions of orogenic belts were also discussed by Downing & Coward (1981) in the Damaran belt of Namibia. Following the proposals made by Elliott (1976), Coward & Potts (1983) demonstrated that intense shear strains (γ_1) may develop at the frontal tips to thrusts and shear zones, where layer-parallel shortening will lead to folding at a high angle to transport (Fig. 1a and 2). Coward & Potts (1983) also demonstrated that lateral tips are marked by additional differential shear strains (γ_2), resulting in asymmetric buckle folds with axes oblique or even subparallel to the direction of flow (Fig. 1b). Differential shear in mylonite zones may thus generate variable fold patterns in adjacent rocks (Fig. 1c); (e.g. Evans & White 1984, fig. 11) and may be related to transient flow perturbations that develop at different scales. The resulting folds and associated structures may therefore also display differing scales, differing relative timing relationships, differing orientations in terms of fold trend, and differing geometries in terms of fold shape and vergence. Many of these criteria have in the past been used to separate fold 'phases' in a rigorous framework (i.e. F_1, F_2, F_3, etc). Flow perturbations models cast doubt on the validity and correlation of fold sequences within high-strain zones on geometric grounds and without recourse to independent methods of testing, such as isotopic dating.

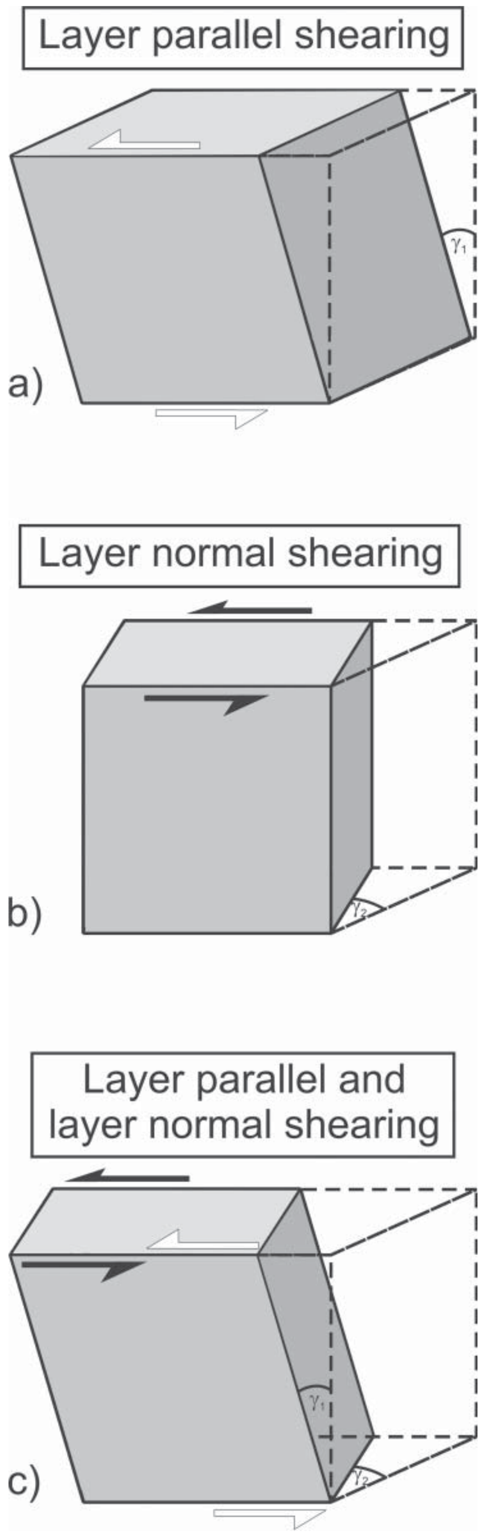

Fig. 1. (**a**) Shear strains (γ_1) associated with layer-parallel shearing may develop at the frontal tips to thrusts and shear zones, resulting in folding at a high angle to transport. Layering lies approximately parallel to the base of the cube. (**b**) Differential shear strains (γ_2) associated with layer-normal shearing may develop at lateral tips to thrusts and shears, resulting in asymmetric buckle folds with axes oblique or even subparallel to the direction of flow. (**c**) Combinations of layer-parallel (γ_1) and layer-normal (γ_2) shearing may develop in mylonite zones, resulting in variable fold patterns in adjacent rocks. Modified from Coward & Kim (1981) and Coward & Potts (1983).

This paper reviews the concept of flow perturbations, and in particular the role of differential shear in the generation of flow cells with different shapes. These models are then tested using a case study from the Caledonides of northern Scotland, where flow perturbation folds display markedly different geometric relationships with hinge trends varying through more than 90°. Various distinguishing criteria and geometric consequences are highlighted from flow perturbations in both contractional and extensional settings, followed by a discussion of flow folding and its relationship to the transport direction.

Synshearing flow folds

Localized perturbations in flow within a shear zone may result in a relative acceleration (surging flow) or deceleration (slackening flow) when compared with the 'background' velocity of the adjacent flow (Fig. 2). Fold culminations are associated with surging flow, with an arc of hinge-line curvature that closes in the direction of transport (Fig. 2a). Depressions are marked by slackening flow, with an arc of hinge-line curvature that opens in the transport direction (Fig. 2b). Within each type of flow cell, localized areas of relative deceleration will generate folds, whereas locally accelerating flow results in extensional shear bands dipping in the flow direction and describing convex and concave arcs in surging and slackening flow cells, respectively. The leading edge of surging flow cells is marked by decelerating flow, whereas the trailing edge is associated with accelerating flow. The reverse pattern occurs in slackening flow cells (Fig. 2b).

The flanks of the flow cells are associated with differential (sinistral or dextral) shear. In both surging and slackening flow cells, sinistral shear generates fold traces clockwise of the flow direction, whereas dextral shear creates anticlockwise-trending folds. The resulting arcuate folds display a concave fold trace in surging flow and convex trace in slackening flow, both of which are bisected by the flow direction. In both surging and slackening flow, folds developed at a high angle to transport will verge in the flow direction. However, transport-subparallel folds developed on the flanks may verge towards the outer edges (surging flow), or towards the inner centre (slackening flow), resulting in markedly different vergence patterns around culmination or depression traces (Fig. 2a and b). Associated fold facing shows a distinct convex arc towards the outer edge of the cell in surging flow, and a concave facing arc towards the centre of slackening flow cells. Thus, culmination or depression surfaces are marked by reversals in the polarity of structural facing, minor fold limb vergence, and fold hinge–transport lineation obliquity (Fig. 2a and b). Fold hinges trending clockwise of transport represent sinistral shear and those trending anticlockwise result from dextral shear. A general description of the regional geological setting of the case study area is provided below, prior to a detailed analysis and interpretation of the highly variable fold patterns.

Regional setting: Caledonian Moine Nappe, Sutherland

The regional geology of NW Scotland is dominated by structures generated during the Early Palaeozoic Scandian phase of the Caledonian Orogeny (*c.* 430 Ma). The most important of these structures is the ESE-dipping Moine Thrust and associated ductile thrusts, such as the Sgurr Beag–Naver Thrust (Fig. 3); (see Strachan *et al.* 2002, for a review). The case study area, centred on the Kyle of Tongue on the north coast of Sutherland, comprises Late Archaean acidic orthogneiss (Lewisian) that forms a basement to Neoproterozoic Moine psammites and subordinate pelites that contain S_1 fabrics and minor F_1 folds, although major D_1 structures are absent (Fig. 3; see Holdsworth *et al.* 2001 for a full review). Structurally, the area is dominated by a D_2 Caledonian ductile thrust stack comprising the Achininver, Ben Hope and Dherue thrusts, together with numerous subordinate ductile thrust imbricates, all containing abundant top-to-the-WNW shear criteria (Fig. 3; Holdsworth *et al.* 2001). Throughout the area, the gently east-dipping regional foliation (S_n) is a bedding-subparallel fabric that intensifies into broad zones of platy mylonite, marking (D_2) ductile thrusts formed at mid-crustal depths (greenschist–amphibolite facies) (Holdsworth 1989; Holdsworth & Grant 1990; Holdsworth *et al.* 2001; Fig. 3). Within the plane of the foliation, a pronounced mineral lineation (L_n), defined by mica together with elongate quartz and feldspar aggregates, plunges gently towards the east directly down the dip of the foliation and is considered to define the trend of tectonic transport (Fig. 4a). Associated (F_2) folds are typically rotated into near parallelism with L_n and define highly curvilinear sheath fold geometries on all scales (Holdsworth 1989; Alsop & Holdsworth 1999, 2004*c*).

The ductile thrusts and associated foliation (S_n) have, during progressive deformation, been folded by kilometre-scale open (F_3) folds that form either subparallel to or at a high angle to the trend of tectonic transport. These major upright

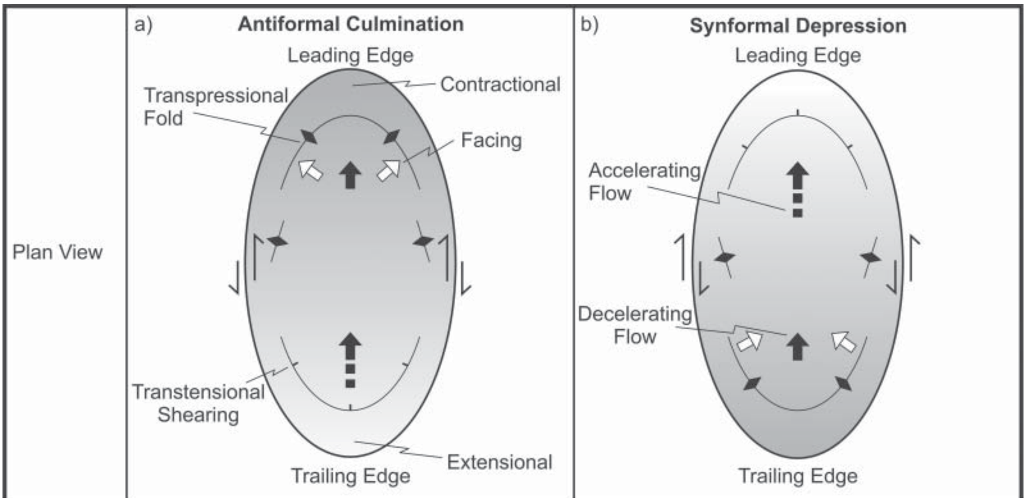

Flow Type	**Surging Flow**	**Slackening Flow**
Flow Pattern	Leading edge - Decelerating flow Trailing edge - Accelerating flow	Leading edge - Accelerating flow Trailing edge - Decelerating flow
Deformation Pattern	Leading edge - Contractional folds Trailing edge - Extensional shears	Leading edge - Extensional shears Trailing edge - Contractional folds
Fold Trace Pattern	Concave fold trace bisected by decelerating flow at leading edge	Convex fold trace bisected by decelerating flow at trailing edge
Fold Trace Pattern - Flanks	Fold traces clockwise of flow related to differential sinistral shear Fold traces anticlockwise of flow related to differential dextral shear	Fold traces clockwise of flow related to differential sinistral shear Fold traces anticlockwise of flow related to differential dextral shear
Fold Vergence Pattern	Folds verge in flow direction at leading edge and towards outer edges on flanks	Folds verge in flow direction at trailing edge and towards inner centre on flanks
Fold Facing Pattern	Convex fold facing arc towards outer edge of flow cell	Concave fold facing arc towards inner centre of flow cell
Shear Pattern	Convex extensional shears dipping in flow direction and bisected by accelerating flow	Concave extensional shears dipping in flow direction and bisected by accelerating flow

Fig. 2. Summary figure highlighting fold and fabric geometries associated with flow perturbation folding. Antiformal culminations are associated with surging flow (left-hand column) whereas synformal depressions are marked by slackening flow (right-hand column). Locally decelerating flow (solid black arrows) results in contractional flow-normal folding, whereas layer-parallel extension associated with locally accelerating flow (broken black arrows) generates extensional shear bands. The flanks of the flow cells are marked by sinistral or dextral layer-normal shear, which results in folds initiating clockwise or anticlockwise to flow, respectively. Arcuate fold trace patterns are marked by variable fold-facing directions (open arrows). (See text for further discussion).

folds define culmination or depression surfaces that root downwards onto underlying thrusts, and have previously been attributed to perturbations in ductile flow within underlying mylonite zones (Holdsworth 1990; Alsop & Holdsworth 1993, 2002, 2004*b*; Alsop *et al*. 1996; Holdsworth *et al*. 2007; Fig. 3).

Major medial (culmination or depression) surfaces typically form orthogonal to the foliation surface and are parallel to transport. Associated (F_3) fold hinges define arcuate traces that may vary from largely transport-parallel to transport-normal. F_3 fold traces, developed subparallel to the transport direction (marked by

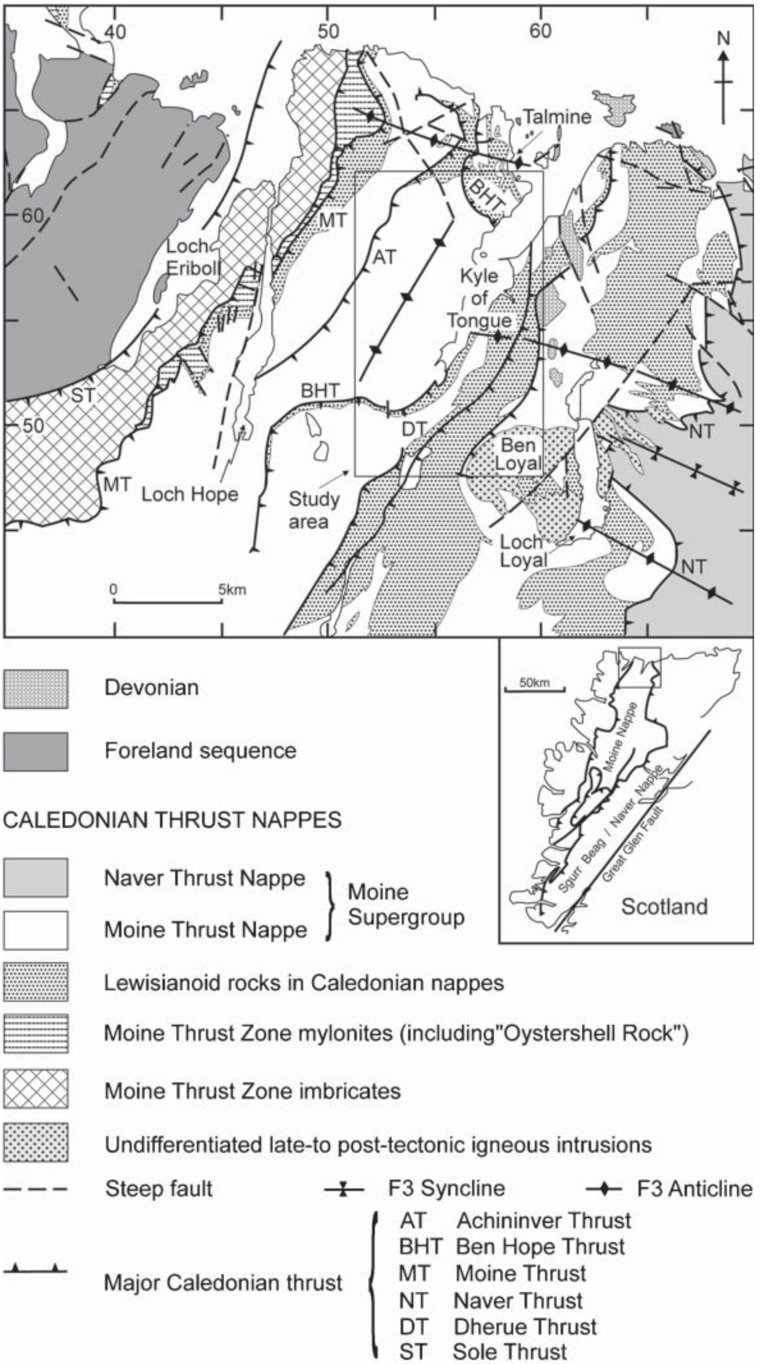

Fig. 3. Simplified geological map of the Moine and Naver nappes in the Kyle of Tongue area, highlighting the location of the study area (see also British Geological Survey 1997, 2002). Major NW- to WNW-directed Caledonian ductile thrusts that carry reworked Lewisian in the hanging wall are shown with solid barbs. These thrusts are subsequently folded by major upright folds, trending either subparallel or at high angles to tectonic transport. The reference grid relates to the UK National Grid, with the map area falling within the NC prefix quadrangle. The inset shows the location of the map in relation to Scotland, with the Moine and Naver nappes being carried on Caledonian thrusts.

the mineral lineation), are observed to the east of the Kyle of Tongue, where the Naver Thrust is markedly deflected by SE-trending folds that root downwards onto the underlying Ben Blandy Shear Zone and Dherue Thrust (Figs 3 and 4a; Alsop *et al.* 1996; Holdsworth *et al.* 2001). In the Talmine area, at the northern end of the Kyle of Tongue, transport-parallel F_3 folding arches the Ben Hope and Achininver thrusts, together with the underlying Moine Thrust, resulting in a marked thickening of the associated mylonites (Alsop & Holdsworth 1993, 2002, 2004*b*; Figs 3 and 4a). The planar geometry of the structure underlying the mylonites in the hinge of the culmination suggests that it has not been affected by the flow perturbation folding and may have acted as the local basal décollement to the deformation (Alsop *et al.* 1996; Holdsworth *et al.* 2001; Alsop & Holdsworth 2002).

F_3 fold traces, developed at a high angle to transport and trending NE–SW, are observed immediately to the west of the Kyle of Tongue (Fig. 3). The trace of the Ben Hope Thrust is markedly deflected by this folding, resulting in a pronounced swing in strike where it arches around the gentle culmination. The overall arching and folding of the Ben Hope Thrust and associated contacts results in the orientation of the mean regional foliation (S_n) and lineation (L_n) varying around the closures at the northern and southern terminations of the major transport-normal fold (Fig. 4a–d). This major eye-shaped closure thus governs the trend of the regional foliation (S_n) and mineral extension lineation (L_n)

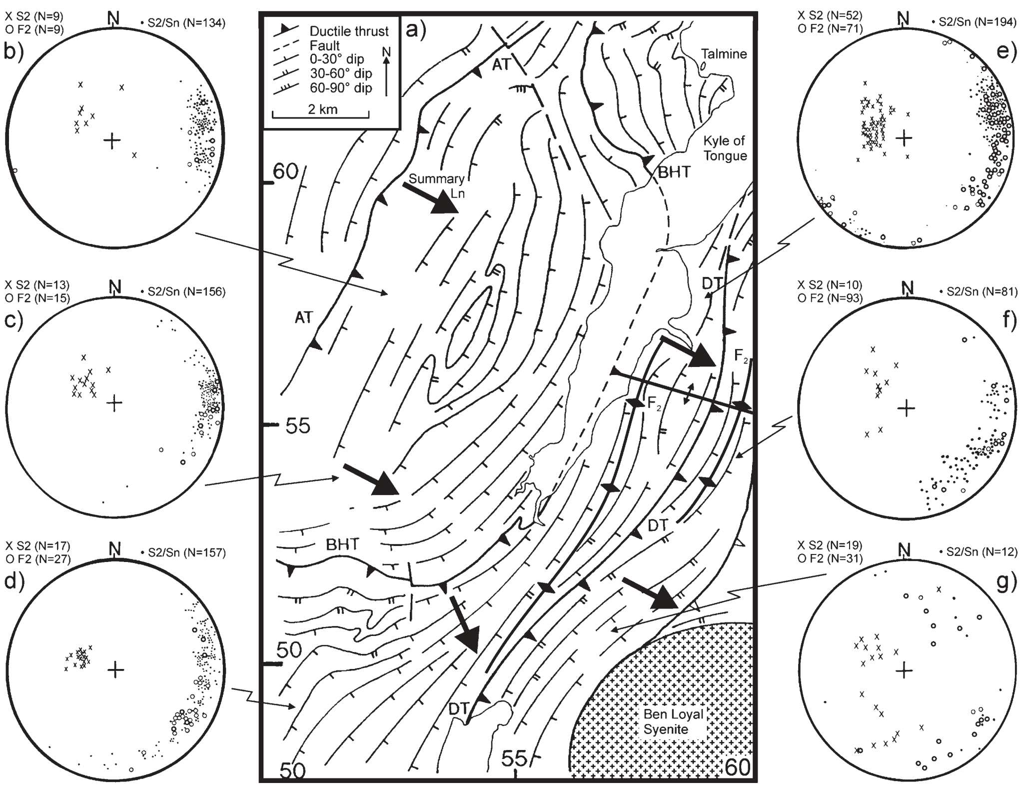

Fig. 4. (**a**) Simplified structural map of the Kyle of Tongue area, highlighting the location of the Achininver (AT), Ben Hope (BHT) and Dherue (DT) thrusts. The trace of the regional foliation (S_n) is marked and typically dips gently to moderately towards the SE. Summary lineation (L_n) arrows are also shown and plunge gently to the SE. Major F_2 antiforms, on either side of the Dherue Thrust, are marked on the eastern side of the map. Equal area lower hemisphere stereographic projections of F_2 fold hinges, S_2–S_n intersection lineations and poles to axial-planar S_2 are shown from the western (**b–d**), and eastern sides (**e–g**) of the Kyle of Tongue. F_2 fold hinges and S_2–S_n intersection lineations define stereographic girdle patterns that are consistent with large-scale curvilinear folding. (See text for further discussion.)

developed immediately to the west of the Kyle of Tongue, and has previously been attributed to F_3 folding in the area (Alsop & Holdsworth 1993). The underlying Achininver Thrust appears to maintain a constant NE–SW strike and is unaffected by these transport-normal folds, which are therefore considered to root downwards onto this planar structure (Fig. 3). Thus, the Achininver Thrust appears to act as a basal décollement for the transport-normal folding west of the Kyle of Tongue, but is itself folded by the transport subparallel folding of the Talmine area, which roots downward into the Moine Thrust Zone mylonites (Fig. 3). The folding in both areas deforms the main foliation (S_n) and lineation (L_n) and is therefore considered to be of broadly similar (F_3) age. The differing relative timing of F_3 folds and individual ductile thrusts reflects the complexity of flow cells within ductile imbricates and additionally highlights the progressive propagation of thrusting and associated deformation towards the foreland (WNW), so that folds rooting down into structurally lower thrusts generally formed later in the sequence.

Patterns of folding in the Moine Nappe

It is important to assess whether the differing trends of F_3 folds can be attributed to the influence of earlier F_2 structures. A detailed geometric analysis of the (F_2) sheath folds and (F_3) syn-shearing flow perturbation folds on either side of the Kyle of Tongue is therefore presented below.

F_2 folding

Throughout the Kyle of Tongue study area, the axes of tight to isoclinal F_2 folds generally plunge gently towards the east, and define incomplete stereographic girdle patterns (Fig. 4). An intense fabric (S_2), developed axial-planar to F_2 folds, typically dips gently towards the ESE and forms an S_2–S_n intersection lineation with the regional foliation (S_n). In the northern part of the area to the west of the Kyle of Tongue, S_2–S_n plunges gently towards the east and is typically developed anticlockwise of the associated F_2 fold hinges (Fig. 4a–c). Such relationships are consistent with clockwise rotating fold hinges (see Alsop & Holdsworth 1999, 2004*c*, for reviews). In the southern part of this area, F_2 hinges and S_2–S_n intersections display greater variability of trends with increased SE- and south-directed plunges, resulting in a pronounced stereographic girdle (Fig. 4d). Increasing south- and SE-directed plunges (which are also displayed by L_n) may be a consequence of the subsequent overall arching on the southern flank of the F_3 culmination that dominates the area.

The pronounced transport-normal F_3 folding is largely absent in the region east of the Kyle of Tongue, as shown in Fig. 4, and this provides an opportunity to study F_2 fold patterns that are little affected by subsequent arching. In the north, both F_2 hinges and S_2–S_n generally plunge gently towards the ENE and define incomplete gently east-dipping stereographic girdles, subparallel to the axial-planar S_2 fabric (Fig. 4e). Similar patterns are observed farther south, although with a greater variability in trends, which typically become more SE plunging (Fig. 4f and g). This F_2 folding is associated with a major curvilinear antiform, cored by Lewisian gneiss, which is developed immediately to the east of the Kyle of Tongue (Fig. 4a; Holdsworth 1989; Holdsworth *et al.* 2001). The WNW-trending culmination of this F_2 fold broadly corresponds to the variation in F_2 fold patterns noted above and is also clearly marked by the outcrop of a ‘core region’ of more acidic Lewisian orthogneiss mapped within the basement inlier (British Geological Survey 1997; Holdsworth *et al.* 2001). It is notable that this culmination also coincides with the continuation along-transport of the major F_3 culmination described from the western side of the Kyle of Tongue (Fig. 4a). This may suggest a degree of ‘inheritance’ across the intervening Ben Hope Thrust.

F_3 folding

Although F_3 folds and fabrics clearly deform the earlier F_2 structures, they may be considered as being related to progressive deformation during D_2 thrusting because of their similar top-to-the-west kinematics and close association with D_2 thrusts (for further details see Holdsworth 1990; Alsop & Holdsworth 2004*b*). Throughout the study area, F_3 folds typically form close to tight buckles, which deform the main regional foliation (S_n) and associated extension lineation (L_n). A crenulation cleavage (S_3) is axial-planar to F_3 folds and typically is more steeply dipping than the adjacent foliation.

To the west of the Kyle of Tongue, F_3 folds display close to tight geometries, display overall west-directed vergence and, in the northern part of the area, plunge gently towards both the NNE and SSW (Fig. 5a and b). The associated axial-planar S_3 fabric is NNE-striking and dips moderately towards the ESE, steeper than S_n. Farther south, F_3 folds increasingly display SSE-directed plunges off the southern flanks of the regional F_3 whaleback, whereas the axial-planar S_3 fabric consistently dips moderately towards the ESE

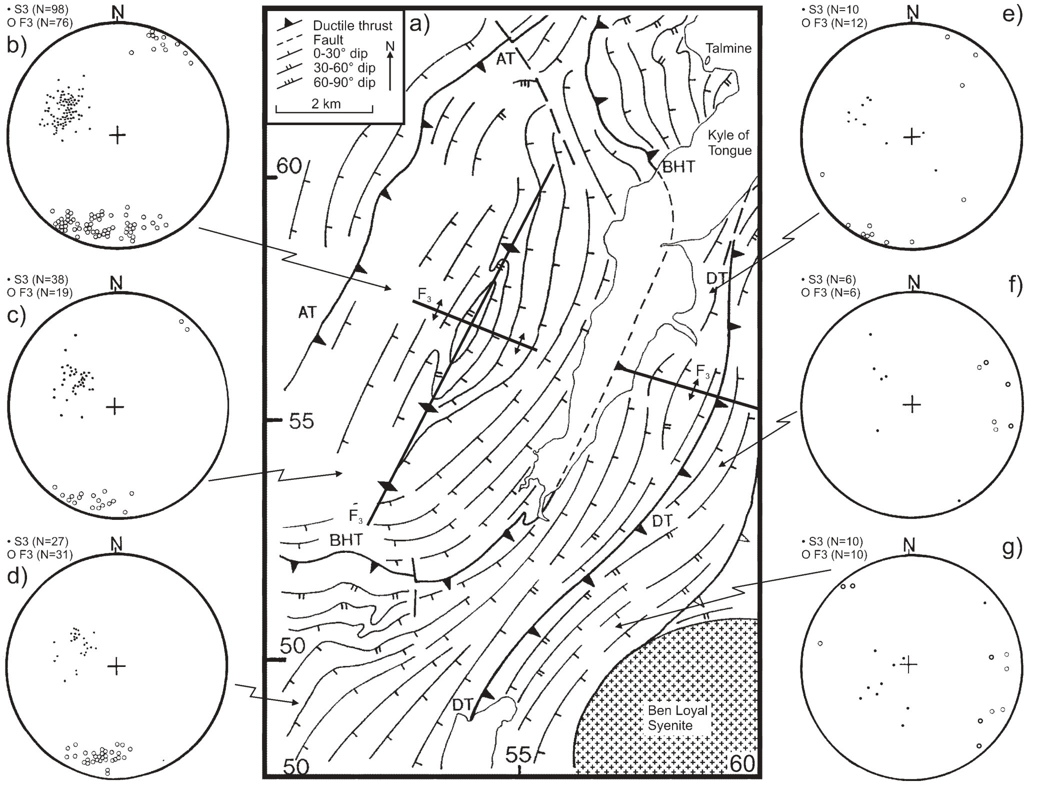

Fig. 5. (**a**) Simplified structural map of the Kyle of Tongue area, highlighting the location of the Achininver (AT), Ben Hope (BHT) and Dherue (DT) thrusts. The trace of the regional foliation (S_n) and Ben Hope Thrust displays a pronounced swing in strike where it arches around the gentle NE-trending F_3 antiform to the west of the Kyle of Tongue. Major F_3 culminations on either side of the Kyle of Tongue are aligned parallel to tectonic transport. Equal area lower hemisphere stereographic projections of F_3 fold hinges and poles to axial-planar S_3 are shown from the western (**b**–**d**), and eastern sides (**e**–**g**) of the Kyle of Tongue. (See text for further discussion.)

(Fig. 5c and d). Overall, to the west of the Kyle of Tongue, there is an absence of measured F_3 hinge trends along a 106° arc, centred about the ESE-plunging extension lineation defining tectonic transport. As this arc is precisely and symmetrically bisected by mean L_n, it suggests that the pattern of F_3 folds represents an actual distribution, rather than a coincidental artefact of sampling and exposure.

To the east of the Kyle of Tongue, close to tight F_3 folds display ESE trends, subparallel to L_n, and no distinct arc lacking F_3 folds is observed (Fig. 5e–g). F_3 folds display variably oriented axial planes that define an imprecise stereographic girdle pattern rather than the clustered distribution observed to the west of the Kyle of Tongue (Fig. 5e–g). It is notable that the pole to this best-fit axial-planar girdle broadly corresponds to the transport lineation (L_n) (see below and Alsop & Holdsworth 2002).

F_2 and F_3 topological relationships

A further analysis of F_2 and F_3 data is presented on fabric topology plots (FTPs) that directly compare angles between sets of planar and linear data (see Alsop & Holdsworth 2004*c*, for a review). In dip-slip thrust systems, the asymmetry of minor F_2 and F_3 folds may be described as Z, S or neutral verging M when viewed down-plunge. In addition, the obliquity of minor F_2 fold hinges to the mineral lineation (L_n), defining tectonic transport, may be described as clockwise or anticlockwise when viewed from above. This distinction is less meaningful in F_3 folds that are typically transport-normal and are therefore described as Z or S folds that are broadly west- or east-verging.

The angle between F_2 hinges and L_n displays a strong positive relationship with the trend of F_2 hinges, reflecting the variability of F_2 hinges about the relatively constant mineral lineation (L_n; Fig. 6a, b and e). The trend of F_2 hinges strongly correlates with the F_2 pitch on associated axial planes, with most hinges pitching between 30° and 120° (Fig. 6c and f). The pitch of F_2 hinges is also seen to vary in relation to the strike of F_2 axial planes, with hinges trending clockwise of L_n typically pitching at greater angles (Fig. 6d and g). Thus, the development of Z and S minor F_2 fold hinges both clockwise and anticlockwise of L_n suggests that both the upper and lower limbs of larger-scale F_2 sheath folds have been sampled (see Alsop & Holdsworth 2004*c*). In addition, F_2 data from both the west and east of the Kyle of Tongue display similar overall patterns on the FTPs, indicating that no consistent geometric differences exist in F_2 folds and fabrics across the Kyle of Tongue.

In contrast, analysis of F_3 folds on FTPs reveals distinctly different patterns on either side of the Kyle of Tongue. On both the eastern and western side, the angle between F_3 hinges and L_n displays a strong positive relationship with the trend of F_3 hinges, reflecting the variability of F_3 hinges about the relatively constant mineral lineation (L_n; Fig. 7a, b and e). However, the data from the western side typically display angles of $>60°$ between fold hinges and the lineation, whereas the eastern side is marked by angles of $<60°$. These distinct differences in the trend of F_3 fold hinges across the Kyle of Tongue are also clearly reflected in the values of F_3 hinge pitch on axial planes (Fig. 7c and f). The pitch of F_3 fold hinges on associated axial planes is less clearly related to the strike of axial planes than that of the F_2 folds (Fig. 7d and g). This weaker F_3 correlation reflects the wide range of hinge trends that are developed within the variably oriented axial planes. Thus, the F_3 topological patterns observed from the east of the Kyle of Tongue are similar to those described for F_2 folds from this same area. However, in the region to the west, very different F_3 and F_2 patterns emerge, with NE–SW-trending westerly verging F_3 folds forming a transport-normal whaleback. The relative constancy of F_2 structures on either side of the Kyle of Tongue may suggest that the siting of the major transport-normal F_3 folding is not significantly influenced by any variability or location of pre-existing F_2 structures. These distinct F_2 and F_3 fold patterns across the Kyle of Tongue are now interpreted in terms of flow perturbation models that are briefly reviewed below.

Flow perturbation folding

Folds generated by variations in flow within underlying mylonitic high-strain zones (flow perturbation folds) may define a variety of arcuate fold trace patterns about the transport direction. Velocity (and hence shear strain) gradients parallel to the direction of flow will generate layer-parallel shear (LPS) with the fold hinges initiating at a high angle to transport, whereas gradients in velocity normal to the direction of flow will generate differential layer-normal shear (LNS) with fold hinges oblique or subparallel to transport (Alsop & Holdsworth 2002). Variable combinations of LPS and LNS components will thus generate a variety of distinct arcuate fold patterns described below.

Layer-normal shearing

Flow in which differential LNS is dominant over LPS will generate folds with hinges initiating oblique or even subparallel to flow (Figs 8a and 9a). Culmination or depression surfaces will correspond to reversals in the sense of differential LNS. Differential sinistral LNS will generate anticlockwise vorticity, with Z fold hinges (looking down transport) preserved clockwise of the transport direction, whereas differential dextral LNS will create clockwise vorticity, with anticlockwise-trending S fold hinges (Figs 8a and 9a). Histograms of fold hinge trends will define an oblique bimodal distribution pattern on either margin of the transport (*X*) direction. The obliquity of fold hinge trends about the culmination surface is marked by reversals in the sense of fold facing, which will also define an oblique bimodal pattern on histograms considered typical of flow perturbation folding (e.g. Alsop & Holdsworth 2002, fig. 9) (Figs 8a and 9a). Hinge rotation can be precluded from generating such transport-subparallel cylindrical folds as they possess open–close interlimb angles that would be severely tightened if progressive shear had produced significant rotation of originally transport-normal hinges (see Alsop & Holdsworth 1999, 2004*c*, 2005). The length/width ratio of individual flow cells (measured parallel to flow) within LNS-dominated deformation will typically be >1, with flow cells elongate in the direction of flow.

Layer-parallel shearing

Flow in which LPS is dominant over differential LNS will generate folds that verge in the direction of shear, and initiate with hinges lying at high angles to the flow direction. The transport-subnormal attitude of such folds means they may be susceptible to significant hinge rotations during continued progressive LPS deformation to define parabolic traces about the flow

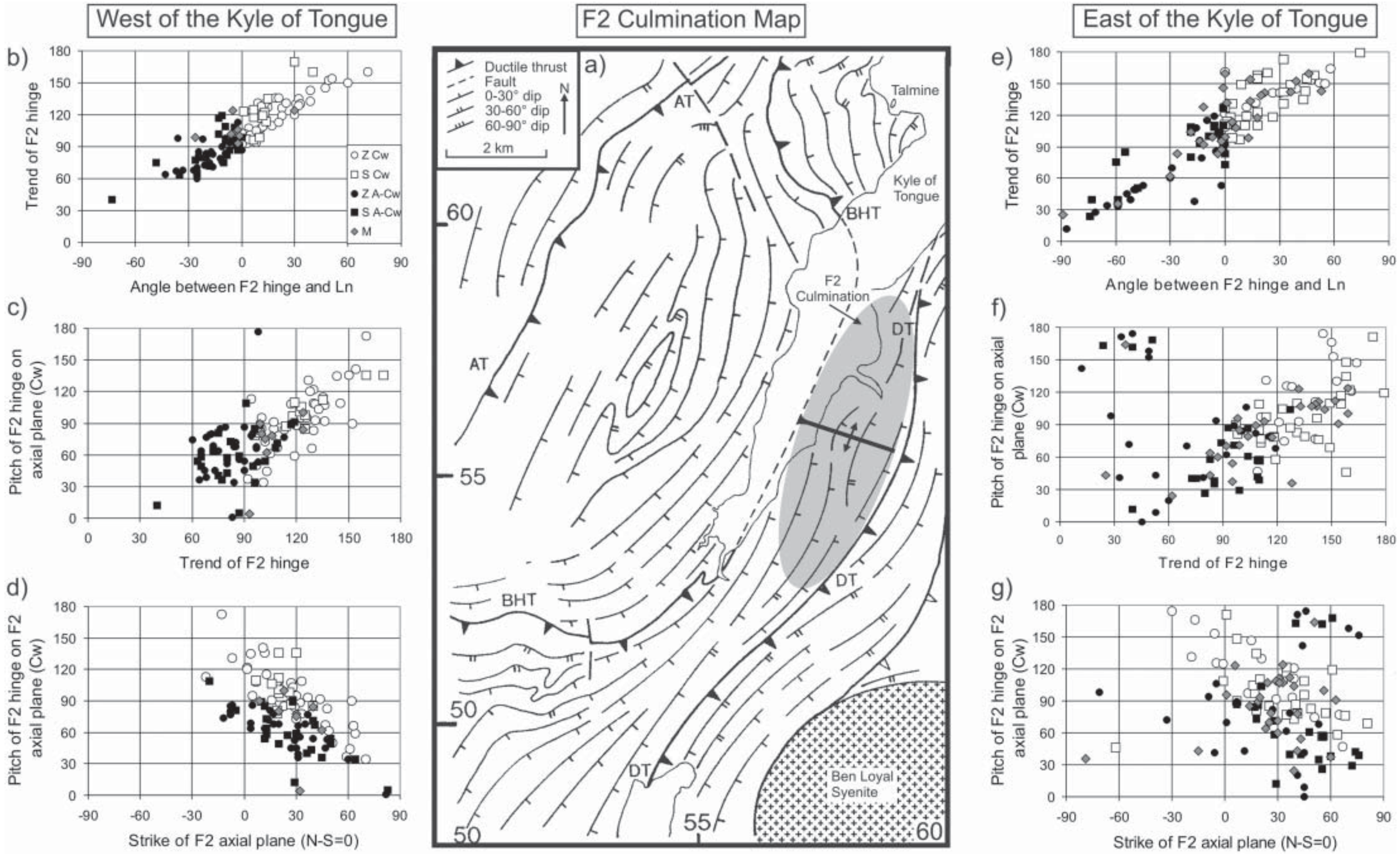

Fig. 6. (**a**) F_2 culmination map showing the location of the major transport-parallel culmination trace to the east of the Kyle of Tongue. The elliptical geometry of the flow cell is schematically shown (tone) and notably corresponds to an F_2 antiform cored by Lewisian gneiss. Fabric topology plots (FTPs) display F_2 fold data, which may be clockwise (open symbols) or anticlockwise (filled symbols) of the adjacent transport lineation from the west (**b**,**c**,**e**) and east (**e**,**f**,**g**) of the Kyle of Tongue. Structures associated with F_2 Z folds (circles), S folds (squares) or M folds (diamonds) may be clockwise or anticlockwise (negative) of L_n (**b**,**e**), whereas the pitch of F_2 fold hinges (**c**,**d**,**f**,**g**) is measured clockwise from axial-planar strike. Whereas F_2 fold trend values are given between 0° and 180°, values of axial-planar strike are displayed for 90° either side of 0° strike, to illustrate more clearly the continuation of geometric trends across the north–south direction. (Refer to text for further details.)

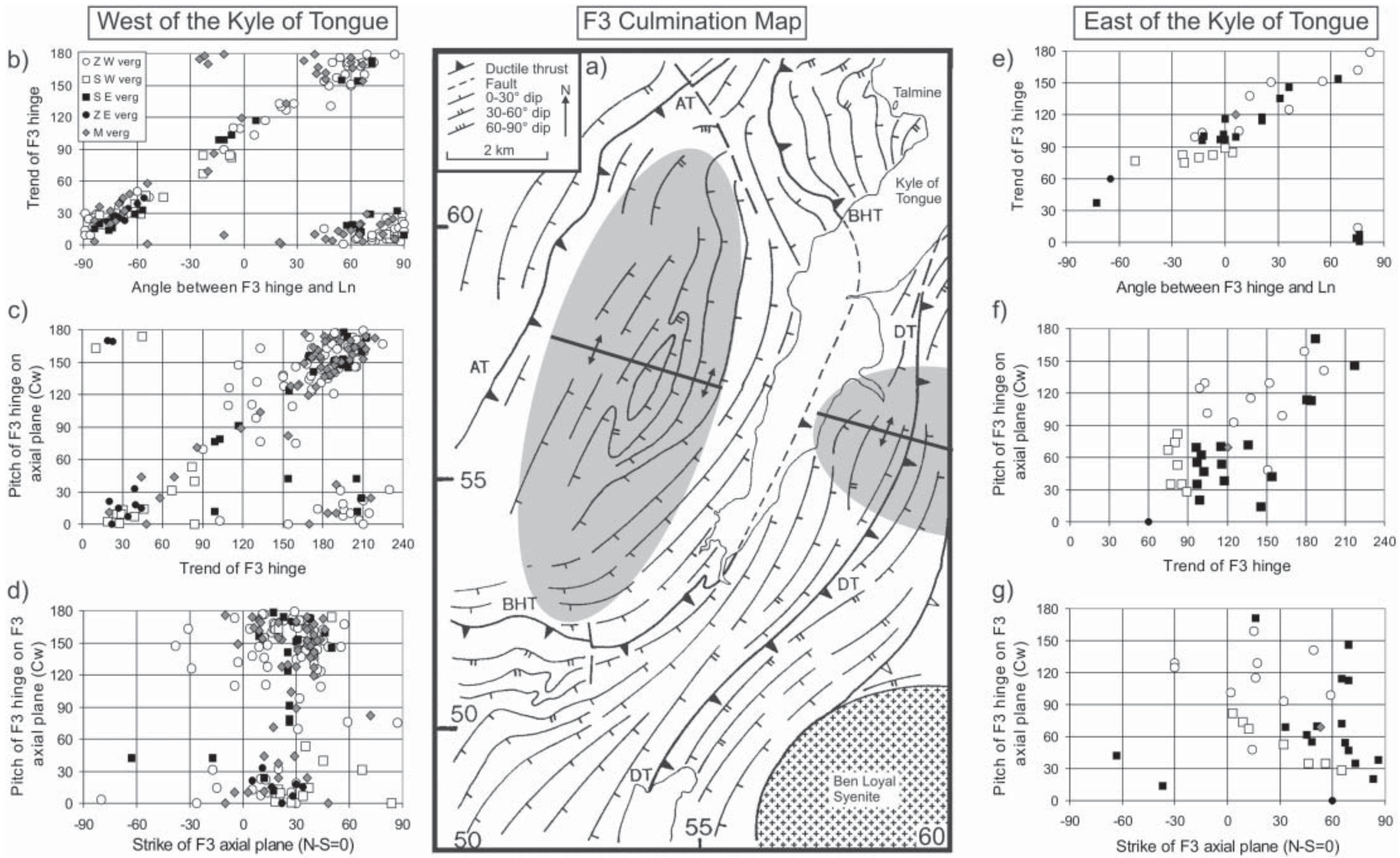

Fig. 7. (**a**) F_3 culmination map showing the location of the major transport-parallel culmination traces to the west and east of the Kyle of Tongue. The elliptical geometry of the flow cells is schematically shown (tone) and displays markedly different trends. Fabric topology plots (FTPs) display F_3 fold data, which may be north- and west-vergent (open symbols), south- and east-vergent (filled symbols) or neutral-vergent (tone) from the west (**b**,**c**,**e**) and east (**e**,**f**,**g**) of the Kyle of Tongue. Structures associated with F_3 Z folds (circles), S folds (squares) or M folds (diamonds) may be clockwise or anticlockwise (negative) of L_n (**b**,**e**), whereas the pitch of F_3 fold hinges (**c**,**d**,**f**,**g**) is measured clockwise from axial-planar strike. Whereas F_3 fold trend values are given between 0° and 240°, values of axial-planar strike are displayed for 90° either side of 0° strike, to illustrate more clearly the continuation of geometric trends across the north–south direction. (Refer to text for further details.)

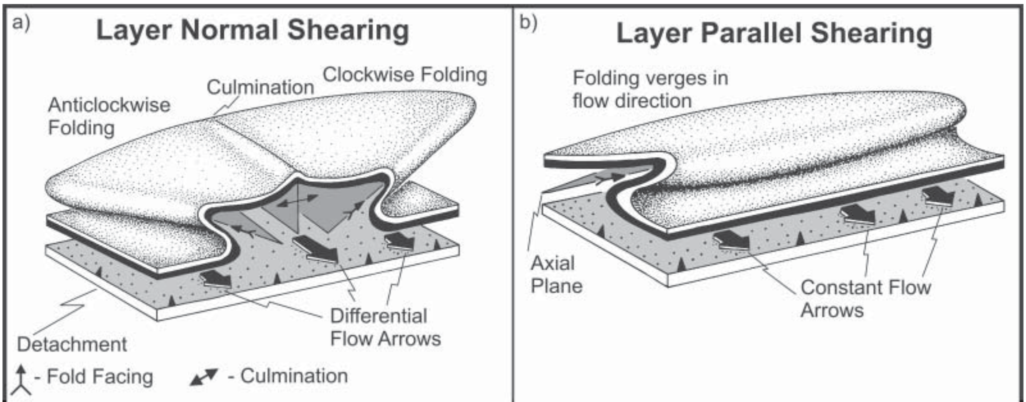

General LNS relationships	**General LPS relationships**
Flow cell ratio >1	Flow cell ratio <1
Ductile equivalent to lateral ramps	Ductile equivalent to frontal ramps
With progressive deformation, folds may evolve into oblique asymmetric folds	With progressive deformation, folds may evolve into curvilinear sheath folds
Arching produces major deflections in strike of overlying layers	Arching produces limited deflections in strike of overlying layers
Fold hinge orientation, vergence and facing	**Fold hinge orientation, vergence and facing**
Cylindrical folds <45° to flow direction	Non-cylindrical folds >45° to flow direction
Reverse asymmetry vergence about flow direction	Normal asymmetry vergence about normal to flow direction
Overall fold vergence at a high angle to flow direction	Overall fold vergence sub-parallel to flow direction
Bimodal fold facing pattern at a high angle to flow direction	Unimodal fold facing pattern sub-parallel to flow direction
Axial-planar orientations	**Axial-planar orientations**
Systematic steepening of axial planes as strike becomes transport-parallel	Systematic steepening of axial planes as strike becomes transport-normal
Z and S fold axial planes intersect parallel to flow direction	Z and S fold axial planes intersect normal to flow direction
M fold hinges and axial planes are sub-parallel to flow direction	M fold hinges and axial planes are sub-normal to flow direction

Fig. 8. Summary figure highlighting fold, fabric and facing geometries associated with flow perturbation folding. Flow perturbation folding dominated by layer-normal shearing (LNS) is shown in the left-hand column, and layer-parallel shearing (LPS) is displayed in the right-hand column. Within LNS, the size of the flow arrow represents the velocity of flow, with dextral shear generating anticlockwise trending folds, whereas sinistral shear is associated with folds trending clockwise of flow. The sense of differential LNS reverses across the culmination surface. The general relationships and geometric consequences of each type of flow pattern are discussed further in the text.

direction (Figs 8b and 9b). The sense of hinge rotation reverses across the medial (culmination or depression) surface, with incomplete anticlockwise rotation preserving fold hinge trends clockwise of the transport lineation and partial clockwise rotation leading to anticlockwise hinge trends (Figs 8b and 9b). Clockwise and anticlockwise fold hinge trends are also marked by reversals in the polarity of fold facing about the culmination surface (Figs 8b and 9b). Histograms of fold hinge trends will define a normalized distribution pattern, centred about the normal to the flow direction, whereas associated fold facing defines a unimodal pattern about the

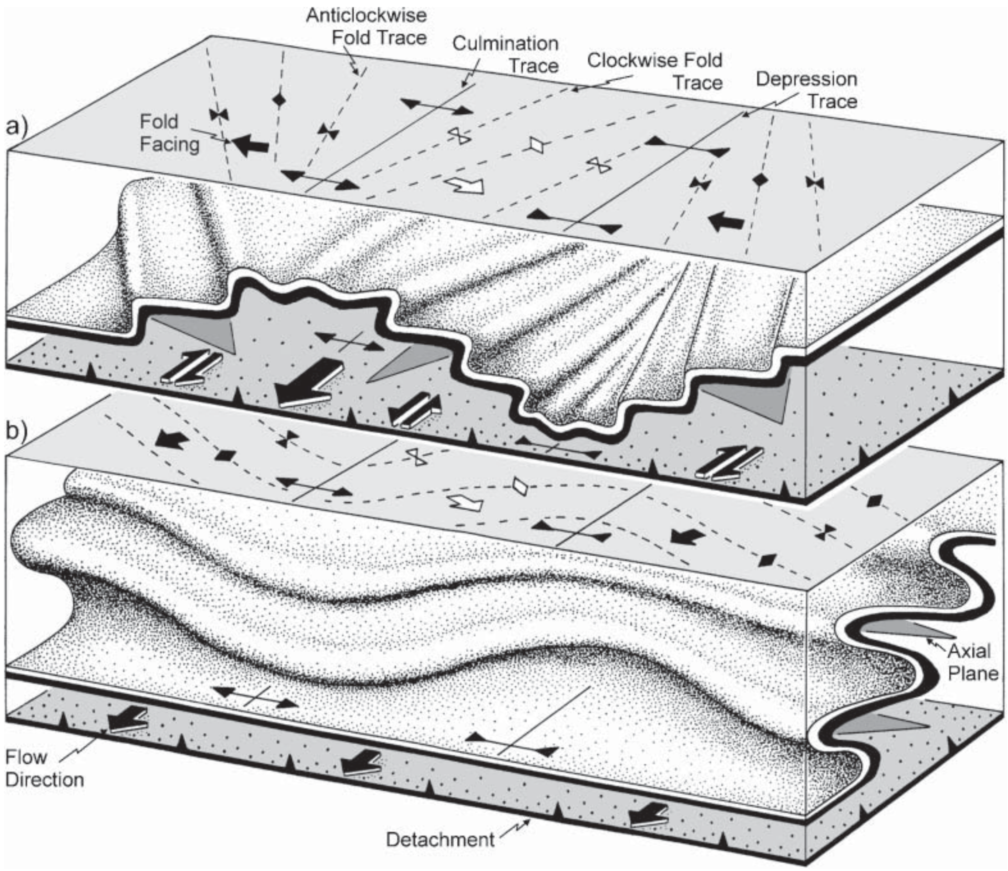

Fig. 9. Schematic 3D illustration of the geometry and orientation of minor structures associated with culmination and depression surfaces in layer-normal shearing (**a**) and layer-parallel shearing (**b**). Culmination surfaces mark regions of surging flow (towards the observer) along the underlying detachment, whereas depression surfaces relate to slackening flow. In (**a**), culminations or depressions separate regions of layer-normal differential dextral shear (shown by half arrows) associated with S folds trending anticlockwise of transport from layer-normal differential sinistral shear relating to Z folds developed clockwise of transport. This results in markedly bimodal facing directions, together with a reversal in the direction of dip of minor axial planes across the culmination or depression surfaces. In (**b**), fold vergence is in the direction of flow, resulting in gentle curvilinear fold traces that typically define facing arcs about the flow direction. (See text for further details.)

flow direction (Figs 8b and 9b). The length/width ratio of individual flow cells within LPS-dominated deformation will typically be <1, with flow cells elongate at high angles to flow.

Summary

During flow perturbation folding, fold traces that define arcuate patterns about the transport direction may be generated by variable components of LPS and LNS, with folding within flow cells balanced by extensional shear bands developed at high angles to transport (Coward & Potts 1983). Flow in which the LPS component dominates will generate flow perturbation folds with fold hinges initiating at high angles to flow, whereas the LNS-dominated flow initiates folding oblique to flow. Thus, close to tight non-cylindrical folds (with hinges typically $>30°$ to flow) reflect LPS whereas close to open cylindrical folds (typically $<30°$ to flow) reflect LNS. Culmination or depression surfaces will correspond to reversals in the sense of differential LNS, with sinistral shear generating Z fold hinges preserved clockwise of the transport direction (looking down plunge) whereas differential dextral LNS will create anticlockwise-trending S fold hinges (Figs 8a,b and 9a,b). The scale and shape of the resultant arcuate fold traces is thus dependent on the degree of partitioning of the two LPS and LNS components and on spatial and temporal variations in rheological parameters, governed by a variety of factors such as strain rate, deformation mechanisms, metamorphic reactions and fluid pressures, together with mechanical anisotropy (see Platt 1983).

Flow perturbation fold patterns may themselves be severely modified and accentuated by continued progressive deformation, resulting in a range of skewed crescentric hinge-lines. Potentially, the parabolic hinge-lines of highly curvilinear folds, previously interpreted as classical sheath folds, could in reality represent one end-member in the continuously evolving hinge morphologies generated by combinations of progressive deformation and (LPS/LNS) perturbations during flow. Progressive deformation (especially that dominated by LPS) will amplify the pre-existing fold arcuate shape and thereby accentuate fabric and facing patterns related to hinge curvature. Increasing components of LNS-dominated flow encourage folds to initiate oblique to transport and to show apparently greater degrees of hinge rotation towards the transport direction for any total shear strain (Coward & Potts 1983). Such LNS-dominated folds will rotate in the same sense for any given differential shear and thereby generate folds that display a consistent sense of obliquity to transport rather than the more variable geometries characteristic of true sheath folds (Alsop & Holdsworth 1999). The exact distribution and frequency of the two transport-parallel and transport-normal fold components is thus governed by (1) the geometry of the flow cell and (2) the role of any subsequent hinge rotation during progressive deformation.

Controls on fold patterns in the Moine Nappe

F_3 fold patterns on either side of the Kyle of Tongue may be interpreted in terms of LPS- and LNS-dominated flow cells described above. To the east of the Kyle of Tongue, F_3 folds are typically developed within 30° of the transport lineation (L_n), suggesting that the area may be dominated by LNS (Fig. 5). Conversely, on the western side of the Kyle of Tongue, the typically high angle (>45°) between L_n and F_3 hinges may reflect a greater component of LPS (see Alsop & Holdsworth 1993). The underlying Achininver Thrust remains unfolded by the major transportnormal folds, suggesting that they may root downwards onto this thrust (Fig. 5). The difference in the LPS and LNS F_3 flow cells on either side of the Kyle of Tongue may reflect a variety of controls, which are discussed below.

Control by structural inheritance

Minor F_2 data collected from both the west and east sides of the Kyle of Tongue are similar in terms of fold hinge trends, axial-planar orientations or mineral lineation trends (L_n; Fig. 4). In both areas, minor F_2 fold hinges define girdles centred about the ESE-plunging L_n. The consistency of minor F_2 folding suggests that it has not significantly influenced subsequent F_3 structures, which display considerable variability across the Kyle of Tongue. In the western area, F_3 folds may have been constrained to develop subparallel to transport with LNS-dominated flow due to the presence of a well-developed linear anisotropy (L_n + near-parallel F_2 axes), which could strongly influence the orientation of subsequent folds and linear fabrics (Watkinson & Cobbold 1981). Interestingly, F_2 hinges are generally more variable in orientation within the F_2 culmination zone to the east of the Kyle of Tongue, whereas the L_n lineation is absent or weak (Holdsworth *et al.* 2001, p. 23).

Control by structural heterogeneity

Major differences in the lithological heterogeneity occur on either side of the Kyle of Tongue. The eastern side displays both acid and mixed Lewisian gneiss, numerous amphibolite sheets and interbanded Moine pelite and psammite, which have been thrust and interfolded at a range of scales. This contrasts starkly with the relatively homogeneous Moine psammites exposed to the west, which lack distinct markers and ductile thrusts (British Geological Survey 1997; Holdsworth *et al.* 2001). In the Talmine and Loch Loyal areas, immediately to the north and east, respectively, a varied and heterogeneous sequence is marked by LNS-dominated deformation (see Alsop *et al.* 1996; Alsop & Holdsworth 2002). This suggests that overall heterogeneity of the system may strongly influence the ability of LNS-dominated flow cells to develop within mylonites and overlying rocks. Heterogeneity (along with fluids and strain rates) may strongly influence the partitioning processes, which will encourage components of LNS flow to develop in the more viscous layers whereas LPS deformation is focused into thinner, less viscous layers (Ridley 1986; Holdsworth 1990; Alsop & Holdsworth 2002). Continued progessive deformation within these weaker units will encourage sheath folds to develop from the originally high-angle LPS folds. The relative heterogeneity of the mixed Lewisian and Moine sequence to the east of the Kyle of Tongue may thus favour LNS-dominated deformation, whereas LPS is encouraged by the relatively homogeneous Moine psammites to the west.

Summary of controls

Unfortunately, the contact between the LPS- and LNS-dominated F_3 flow cells is largely concealed by the Kyle of Tongue. However, at the southern end of the sea loch, south-plunging F_3 folds, suggesting LPS-dominated flow, are developed in both the footwall and hanging wall of the Ben Hope Thrust, which is itself folded on a regional scale by these folds (see Holdsworth 1989, 1990). In this immediate region, the switch from LNS to LPS flow appears to occur across the structurally higher Dherue Thrust (Fig. 7). However, the LNS flow cell to the east of the Kyle of Tongue produces an arching of the Dherue Thrust, and is therefore considered to possibly root downwards onto the underlying Ben Hope Thrust. Thus, LNS- and LPS-dominated F_3 flow cells appear to have different structural relationships to the D_2 Dherue and underlying Ben Hope thrusts.

The relationships described above are to be expected in a foreland-propagating ductile thrust system where ‘younger’ flow cells, rooting onto structurally lower thrusts, will deform the overlying (older) structures. Complexities concerning the relative ages of flow perturbation folds and ductile thrusts are thus developed both across-strike in the Kyle of Tongue area, and along-strike when thrusts are traced farther north into the Talmine area (see section on Regional setting above, Fig. 3). Some general remarks and observations on flow perturbations are presented below, prior to a wider consideration of folding relationships and their applications in contractional and extensional settings.

Geometric fold patterns about flow perturbations

Around flow perturbations there are ordered, scale-independent geometric relationships between fold hinges, fold vergence, fold facing, and fold axial-planar patterns. The exact nature of these relationships will depend on the relative components of LNS- and LPS-dominated flow. The geometric patterns essential to the interpretation of flow perturbation cells are now described in detail and summarized in Table 1.

Fold hinge patterns about flow perturbations

Fold hinges within flow perturbations may form arcuate traces about the flow direction, with sinistral shear on the flanks of the cell generating folds clockwise of transport, whereas dextral shear on the opposing flank will create folds anticlockwise of transport. Within individual perturbations, fold patterns may vary not only in plan view (X–Y plane) on the surface or zone of detachment, but also within the flowing cell itself. For example, folds often display the greatest obliquity to transport on the upper flanks of the perturbation, with the angle of obliquity gradually reducing towards the underlying detachment (e.g. Alsop & Holdsworth 2002). This results in fold trace patterns converging towards the flow direction, both across-strike towards the basal detachment and along-strike towards the culmination or depression surface. This pattern is a consequence of variable strain gradients associated with differential (LNS) shear, possibly coupled with a component of progressive shearing and associated fold-hinge rotation towards the flow direction of the underlying detachment.

Fold vergence patterns about flow perturbations

Flow perturbation folds are marked by minor fold limb vergence, which reflects the sense of short-limb–long-limb asymmetry and may be described in dip-slip systems in terms of down-plunge S, Z and neutral verging M/W folds. The sense of minor fold limb vergence will reverse across-strike when crossing major fold axial planes, and also along-strike when crossing culmination or depression surfaces (for examples, see Alsop & Holdsworth 2002). In most ‘classical’ folds, normal asymmetry vergence is developed in which the short limbs of minor folds rotate in an opposite (antithetic) sense to the major fold limb, which then reverses across the axial plane. Reversals in minor fold asymmetry are observed across-strike when crossing axial planes associated with LPS-dominated folds (Figs 8b and 9b). Such normal asymmetry vergence (i.e. towards antiformal structures) is the exact opposite to that observed in LNS, folds, where short limbs of minor folds rotate in a synthetic sense to the major fold limb (Figs 8a and 9a; Alsop & Holdsworth 2002). Major antiformal culminations and synformal depressions generated during LNS are thus marked by reverse asymmetry vergence, which switches across the culmination or depression surface.

Statistically similar attitudes of pre-existing foliations around major LNS culmination or depression surfaces is simply a consequence of reverse asymmetry vergence where the long limbs of minor folds (with opposing vergence) remain

Table 1. *Summary of topological relationships associated with layer-parallel shearing (LPS) and layer-normal shearing (LNS) in both contractional and extensional settings*

Topological parameter	Observation	Cause	Contractional sense of rotations	Contractional topological relationships	Extensional sense of rotations	Extensional topological relationships	LPS > LNS patterns	LNS > LPS patterns	Effect of progressive deformation on LPS or LNS
(a) *Angle between trend of fold hinge and L_n*	**(a)** reduces with greater deformation	Rotation of fold hinge towards *X*	S hinges rotate Cw Z hinges rotate A-Cw	S hinges trend A-Cw of L_n Z hinges trend Cw of L_n	S hinges rotate A-Cw Z hinges rotate Cw	S hinges trend Cw of L_n Z hinges trend A-Cw of L_n	Broad arc of hinge trends (>45°) to L_n	Cluster of hinge trends subparallel (<45°) to L_n	Greater reduction in (a) in LPS setting
(b) *Angle of pitch of fold hinge on axial plane*	**(b)** increases with greater deformation	Rotation of fold hinge and axial plane towards *X* and *X–Y*, respectively	Z hinges and S axial planes rotate A-Cw S hinges and Z axial planes rotate Cw	S axial plane = Cw hinge pitch Z axial plane = A-Cw hinge pitch	S hinges and S axial planes rotate A-Cw Z hinges and Z axial planes rotate Cw	S axial plane = A-Cw hinge pitch Z axial plane = Cw hinge pitchs	Low values (<45°) of hinge pitch	High values (<60°) of hinge pitch	Greater increase in (b) in LPS settings
(c) *Angle of L_n pitch on axial plane*	**(c)** increases with greater deformation	Rotation of axial plane towards *X–Y* plane	S axial planes rotate A-Cw Z axial planes rotate Cw	S axial plane = Cw L_n pitch Z axial plane = A-Cw L_n pitch	S axial planes rotate A-Cw Z axial planes rotate Cw	S axial plane = Cw L_n pitch Z axial plane = A-Cw L_n pitch	High values (>60°) of L_n pitch	Low values (<45°) of L_n pitch	Greater increase in (c) in LNS settings
(d) *Angle between pitch of fold hinge and L_n*	**(d)** reduces with greater deformation	Rotation of fold hinge and axial plane towards *X* and *X–Y*, respectively	Z hinges and S axial planes rotate A-Cw S hinges & Z axial planes rotate Cw	S hinges pitch A-Cw of L_n Z hinges pitch Cw of L_n	S hinges and S axial planes rotate A-Cw Z hinges and Z axial planes rotate Cw	S hinges pitch Cw of L_n Z hinges pitch A-Cw of L_n	Large differences (>60°) in fold hinge and L_n pitch values	Small differences (<30°) in fold hinge and L_n pitch values	Greater reduction in (d) in LPS setting
(e) *Angle between strike of axial plane and L_n trend*	**(e)** increases with greater deformation	Rotation of axial plane towards *X–Y* plane	S axial planes rotate A-Cw Z axial planes rotate Cw	S axial plane strikes A-Cw of L_n Z axial plane strikes Cw of L_n	S axial planes rotate A-Cw Z axial planes rotate Cw	S axial plane strikes A-Cw of L_n Z axial plane strikes Cw of L_n	Axial planes strike subnormal (>60°) to L_n trend	Axial planes strike oblique (<60°) to L_n trend	Greater increase in (e) in LNS settings
(f) *Angle between strikes of axial plane and S_n*	**(f)** reduces with greater deformation	Rotation of axial plane towards *X–Y* plane	S axial planes rotate A-Cw Z axial planes rotate Cw	S axial plane strikes Cw of S_n Z axial plane strikes A-Cw of S_n	S axial planes rotate A-Cw Z axial planes rotate Cw	S axial plane strikes Cw of S_n Z axial plane strikes A-Cw of S_n	Axial planes strike subparallel (<30°) to S_n trend	Axial planes strike oblique (<60°) to S_n trend	Greater reduction in (f) in LNS setting

Table 1. *Continued*

Topological parameter	Observation	Cause	Contractional sense of rotations	Contractional topological relationships	Extensional sense of rotations	Extensional topological relationships	LPS > LNS patterns	LNS > LPS patterns	Effect of progressive deformation on LPS or LNS
(g) *Acute angle between axial plane and S_n*	**(g)** reduces with greater deformation	Rotation of axial plane towards *X–Y* plane	S axial planes rotate A-Cw Z axial planes rotate Cw	S axial plane = Cw of S_n Z axial plane = A-Cw of S_n	S axial planes rotate A-Cw Z axial planes rotate Cw	S axial plane = Cw of S_n Z axial plane = A-Cw of S_n	Axial planes oblique (<30°) to S_n	Axial planes oblique (<45°) to S_n	Greater reduction in (g) in LNS setting

When viewed from above, fold hinges and axial planes may trend clockwise (CW) or anticlockwise (A-Cw) of the adjacent mineral lineation (L_n) or foliation (S_n). The effects of continued progressive deformation on fold and fabric relationships are also highlighted in the right-hand column. (Refer to text for further details.)

parallel to one another across the culmination surface (see Fig. 9; Alsop & Holdsworth 2002). Clearly, this is the opposite to, and may be used to discriminate from, normal asymmetry vergence patterns, where the long limbs of minor folds are typically rotated, thus resulting in statistically different attitudes on either side of a major fold.

Fold facing patterns about flow perturbations

Fold facing may be defined as 'the direction, normal to the fold hinge, along the fold axial plane, and towards the younger beds' (Shackleton 1958; Holdsworth 1988). In LNS-dominated systems, fold hinges may develop oblique or subparallel to the flow direction, resulting in pronounced bimodal facing patterns at a high angle to transport (Fig. 9a). Minor folds associated with LPS fold limb vergence will typically develop unimodal facing patterns defining gentle arcs, subparallel to the flow direction (Fig. 9b). In both LPS- and LNS-dominated flow cells, the sense of fold facing (measured relative to the constant flow direction) reverses when crossing the culmination or depression surface. Facing patterns may appear highly skewed if the flow cell itself is asymmetric, or if only one flank of the flow cell is sampled. Culminations will be associated with fold facing-arcs directed outwards towards the margins of the perturbation, whereas depressions will be marked by facing directed inwards towards the centre of the cell (Fig. 9, Table 1).

Axial-planar patterns about flow perturbations

Minor fold axial planes display arcuate traces about the flow direction varying from contractional folds developed at high angles to transport, to fold axial planes associated with differential shear striking subparallel to flow on the flanks of the cells. Within LNS-dominated flow cells associated with thrusting, Z fold axial planes strike clockwise of transport and reflect differential sinistral shear, whereas S fold axial planes will strike anticlockwise of transport, indicating differential dextral shear. Neutral verging M/W fold axial planes typically strike at high angles to the flow direction in LPS settings, whereas in LNS-dominated regimes they typically trend subparallel to the flow direction (for examples, see Alsop & Holdsworth 2002). Within such LNS systems, S, Z and M/W axial planes display a systematic steepening as the axial-planar strike becomes transport-parallel. This

3D axial-planar fanning geometry is thus developed about the flow direction (see below), whereas in LPS settings it will occur about the transport-normal direction (Figs 8 and 9).

Axial-planar patterns also vary within the flow cells. Axial planes display the greatest obliquity to the adjacent folation (S_n) on upper flanks of perturbations, whereas the least obliquity to S_n occurs on the lower flanks of the perturbation (Alsop & Holdsworth 2002). Within LNS systems, this results in a convergent axial-planar trace both across-strike towards the underlying basal detachment zone and along-strike across the culmination or depression surface. The rotation of the axial-planar strike towards the trend of the foliation (S_n) is considered to be a consequence of increasing strain towards the underlying detachment zone and thus reflects deformation gradients within the flow cell.

Flow perturbation folds in different environments

The recognition that variable patterns of displacement in thrusts may result in arcuate fold and fault traces was developed in the Canadian Rockies (Elliott 1976) and Moine Thrust Zone (Fig. 10a) (Coward & Potts 1983). This concept has subsequently been widely applied to other thrust belts in which folds apparently root downwards onto detachments (e.g. Allen *et al.* 2001). These techniques and concepts of flow perturbation may, however, also be used in a variety of other settings in which kinematically coherent systems of flow may develop, such as soft-sediment slumps and mud flows. These near-surface settings are gravity-driven and as such will generate dip-slip-dominated systems of deformation related to extensional tectonics.

Soft-sediment slump sheets are an obvious application of the flow perturbation concept (e.g. Woodcock 1979; Farrell 1984; Strachan 2002; Strachan & Alsop 2006) and even display progressive deformation structures reminiscent of mid-crustal curvilinear sheath folds (e.g. Roberts 1989; Fig. 10b). Hansen (1971) applied many of the detailed concepts of flow perturbations to a landslip in which the top 15 cm of tundra sod had moved downslope in Trollheimen, Norway. Similar arcuate fold patterns developed by differential layer-normal shear about the downslope direction are observed in tundra landslips of West Greenland (Fig. 10c). The slipping of material on a shallow detachment surface has also been recognized in snow slides (e.g. Lajoie 1972), where the variability of fold hinge and axial planar orientations was considered a direct consequence of the amount of slide translation. Flow perturbation fold patterns are also developed on a variety of scales in mud flows stemming from mud volcanoes (Fig. 10d). Channelized flow displays drag on either margin, with the degree of finite differential shear (and hence fold trace curvature) therefore increasing down the individual flow (Fig. 10d). Surges within glacial flow have been considered to produce broadly similar features (e.g. Lawson *et al.* 1994; Hambray & Lawson 2000), and salt glaciers and diapirs also display characteristics of variable flow, which may reflect episodic surges associated with variable precipitation (Talbot 1979; Talbot & Jarvis 1984; Talbot & Aftabi 2004). Fold patterns observed in volcanic lava flows (e.g. Fink 1980) may be complicated by the surface cooling of lava, resulting in a thick chilled skin to the flow. This increasingly results in longer-wavelength folds that refold the earlier lava crenulations, resulting in the classic ropy lava with consistent senses of 'twisting' about the flow direction (e.g. Ramsay & Lisle 2000, p. 939).

Many of the above applications of flow perturbation theory are developed in the near surface and are essentially gravity-driven. As such, the deforming material is typically therefore within an extensional system in which downslope (dip-slip) movement predominates. We shall now examine and compare the geometric relationships of flow perturbations developed in such extensional settings with those previously described from contractional settings.

Geometric comparison of flow perturbations in contractional and extensional settings

The sense of hanging-wall movement relative to the flow perturbation detachment has a number of important implications and geometric consequences that will now be briefly reviewed. Folds and fabrics in both contractional and extensional dip-slip systems of deformation are traditionally described by viewing the geometry of such structures in a down-plunge orientation (e.g. McClay 1987). A direct consequence of this is that folds and fabrics are described when looking down-plunge and in the same direction as transport in extensional settings, whereas in contractional settings the down-plunge construction is viewed in a direction exactly opposite to the transport azimuth.

Fold hinge patterns in contraction and extension

A component of fold hinge rotation towards the flow direction is typically demonstrated by

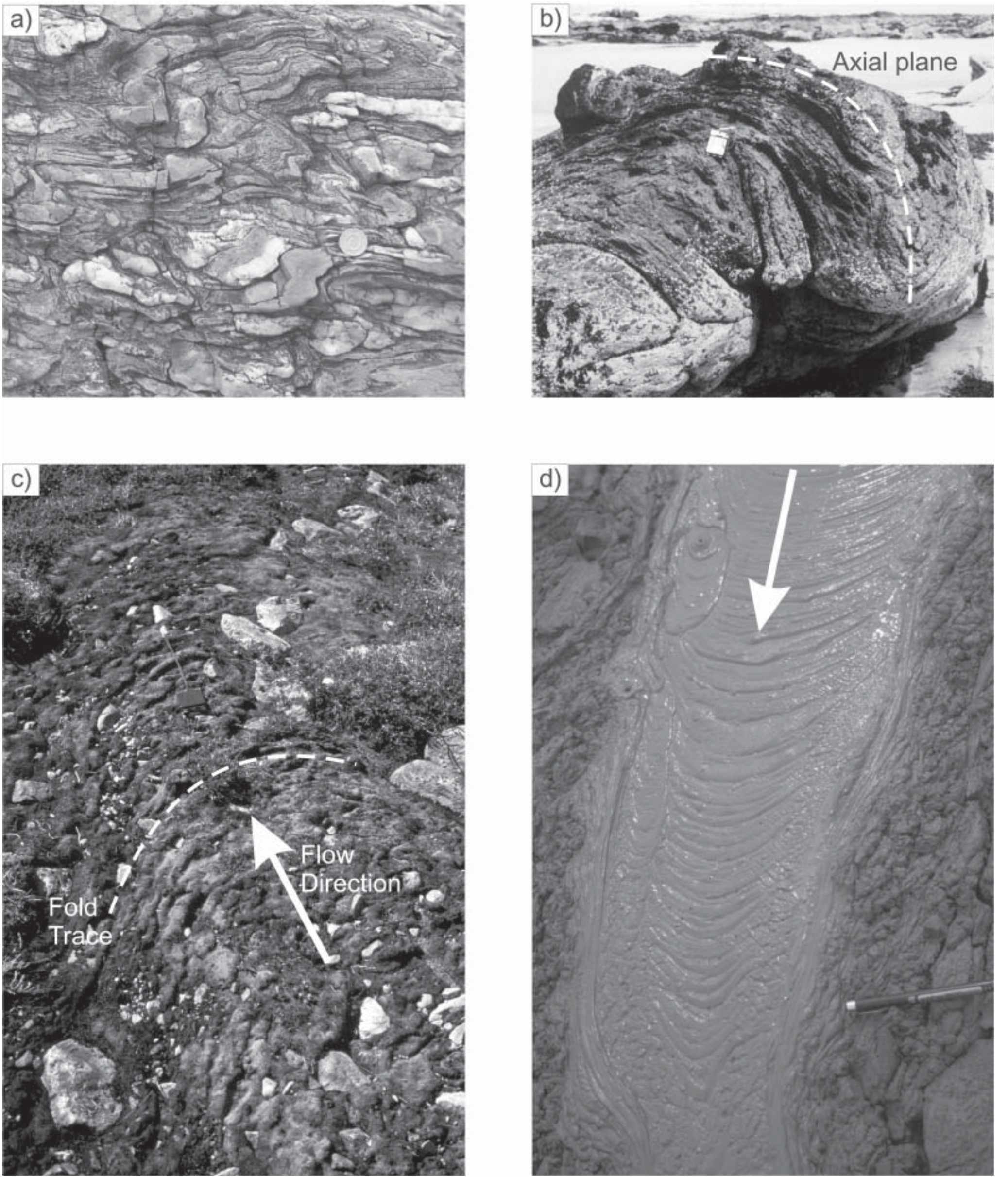

Fig. 10. (**a**) Typical 'F$_3$' flow perturbation folds refolding the mylonitic foliation (S_n) and mineral lineation (L_n) in mylonitized quartzite of the Moine Thrust Zone, Eriboll. (**b**) Gravity-driven near-surface flow perturbations observed in soft-sediment slump sheets in the Jurassic of northern Scotland. These slumps display curvilinear folding and refold patterns, reminiscent of progressive deformation in mid-crustal settings. (**c**) Arcuate fold patterns form in tundra landslips of West Greenland. Differential layer normal shear (away from the observer) occurs about the downslope direction (marked by the compass chord). (**d**) Mud flows stemming from mud volcanoes in Azerbaijan. Channelized flow (towards the observer) displays drag on either margin, with the degree of finite differential shear (and hence fold trace curvature) therefore increasing down the individual flow.

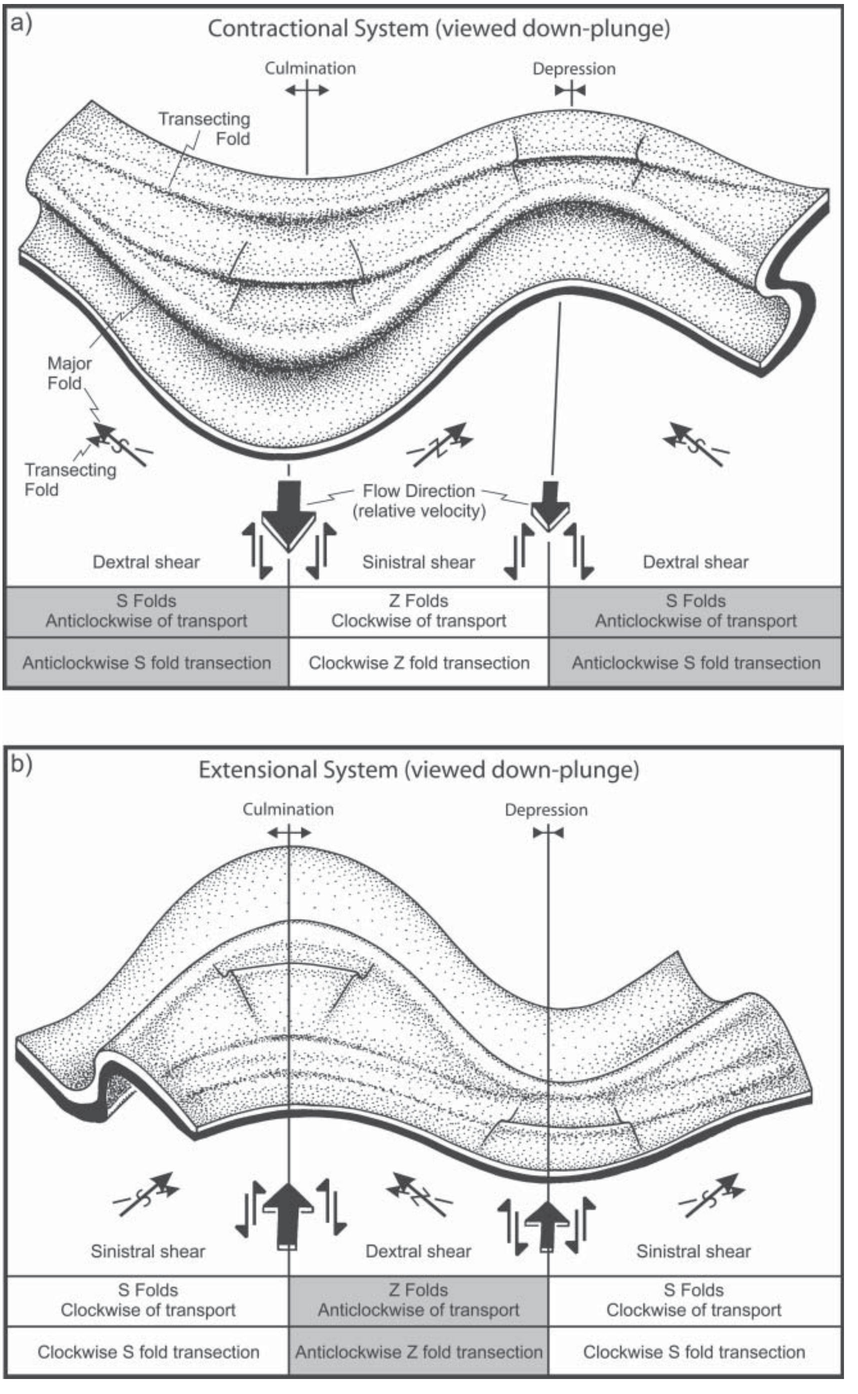

Fig. 11. In both contractional (**a**) and extensional (**b**) systems, differential dextral shear will consistently generate fold hinges anticlockwise of flow (boxes with grey tone), whereas sinistral shear forms folds with a clockwise obliquity. Subsequent folds may overprint older, rotated folds, with the younger folds transecting the older structures with a consistent clockwise or anticlockwise obliquity. Flow directions (and relative velocities) are shown by the black arrows pointing towards the observer in the contractional system (**a**) and away from the viewer in (**b**). (Refer to the text for further details.)

overprinting minor folds on the upper flanks of flow perturbation folds (e.g. Alsop & Holdsworth 2002). These minor folds are considered to relate to the continuing development of the flow perturbation cell, as they consistently display the same sense of asymmetry and obliquity to L_n as the earlier flow folds. However, the overprinting folds make greater angles of obliquity to L_n, such that they display anticlockwise transection of anticlockwise fold hinges and clockwise transection of clockwise fold hinges (Fig. 11). This consistent sense of transection is considered to reflect a degree of hinge rotation during fold amplification and flow cell development.

Differential dextral shear will consistently generate fold hinges anticlockwise of flow in both contractional and extensional settings (Fig. 11a and b). They will, however, display an apparent down-plunge S asymmetry in contractional settings and Z asymmetry in extensional settings. Similarly, differential sinistral shear will consistently generate folds clockwise of flow, which will display apparent Z or S asymmetry in contractional and extensional settings, respectively (Fig. 11a and b). As flow continues, fold hinges may undergo rotation towards the transport direction. The sense of rotation will be governed by the sense of obliquity, with folds generated during dextral and sinistral differential shear undergoing clockwise and anticlockwise rotations, respectively. Subsequent folds may overprint the older rotated folds and will continue to initiate at higher angles to flow. This geometric relationship results in the younger folds consistently transecting the older structures with either a clockwise sense in sinistral shear or anticlockwise sense in dextral shear. These transecting relationships also provide a potential mechanism to determine shear sense.

Fold axial-planar patterns in contraction and extension

The strike of fold axial planes also displays distinct relationships to the trend of flow. Despite the sense of obliquity of S and Z fold hinges reversing from contractional to extensional settings (see Fig. 9a), the sense of axial-planar obliquity relative to the flow direction remains constant (Fig. 12a and b). The strikes of S fold axial planes are consistently anticlockwise of transport, whereas those of Z fold axial planes are clockwise. A consequence of the reversal in fold hinge obliquity and consistency of axial-planar orientations is that the sense in which Z or S fold hinges pitch on their axial planes will reverse from contractional to extensional settings (Fig. 12).

Summary of fabric patterns in contraction and extension

The relationships described above highlight the geometric patterns developed in contractional and extensional systems. Thus, sinistral shear consistently generates fold hinges clockwise of the flow direction, whereas dextral shear generates anticlockwise-trending folds in both contraction and extension. Similarly, the sense of obliquity between the flow direction and the axial-planar strike of Z folds (clockwise) or S folds (anticlockwise) also remains constant in both settings. However, an inherent consequence of the traditional down-plunge view of Z and S fold asymmetry is that S folds appear to be Z folds when viewed from the opposing direction (and vice versa). This geometric artefact results, for example, in the kinematic association of Z fold hinges apparently switching from sinistral to dextral shear in contraction and extension, respectively (Fig. 11a and b). To help alleviate these types of problems, fold hinges whose plunge varies about the horizontal datum may therefore be best described using down-plunge Z and S fold asymmetry coupled where necessary with an additional vergence direction (e.g. west-verging Z fold, etc) as demonstrated by the F_3 folds in the case study area (Fig. 7).

Calculation of flow direction via fold analysis

A variety of techniques have been established, principally in sedimentary environments, that utilize the development of folds to determine the direction of movement. The two existing principal methods for the determination of directions of slumping and hence palaeoslope have been discussed in detail by Woodcock (1979). These are described briefly below prior to a consideration of a recent technique that utilizes the geometric consistency of flow perturbation folds to determine transport.

The mean axis method (MAM)

The mean axis method (MAM) was pioneered by Jones (1940) and takes the (downslope) transport direction as the perpendicular to the calculated mean slump fold axis (which is assumed to verge downslope) (Fig. 13a). Although this technique is simple and easy to apply, the disadvantage is that it fails to allow for differential downslope movements that will result in folds being generated oblique to the palaeoslope. In addition, folds that initiate at high angles to the palaeoslope may subsequently undergo hinge rotation towards

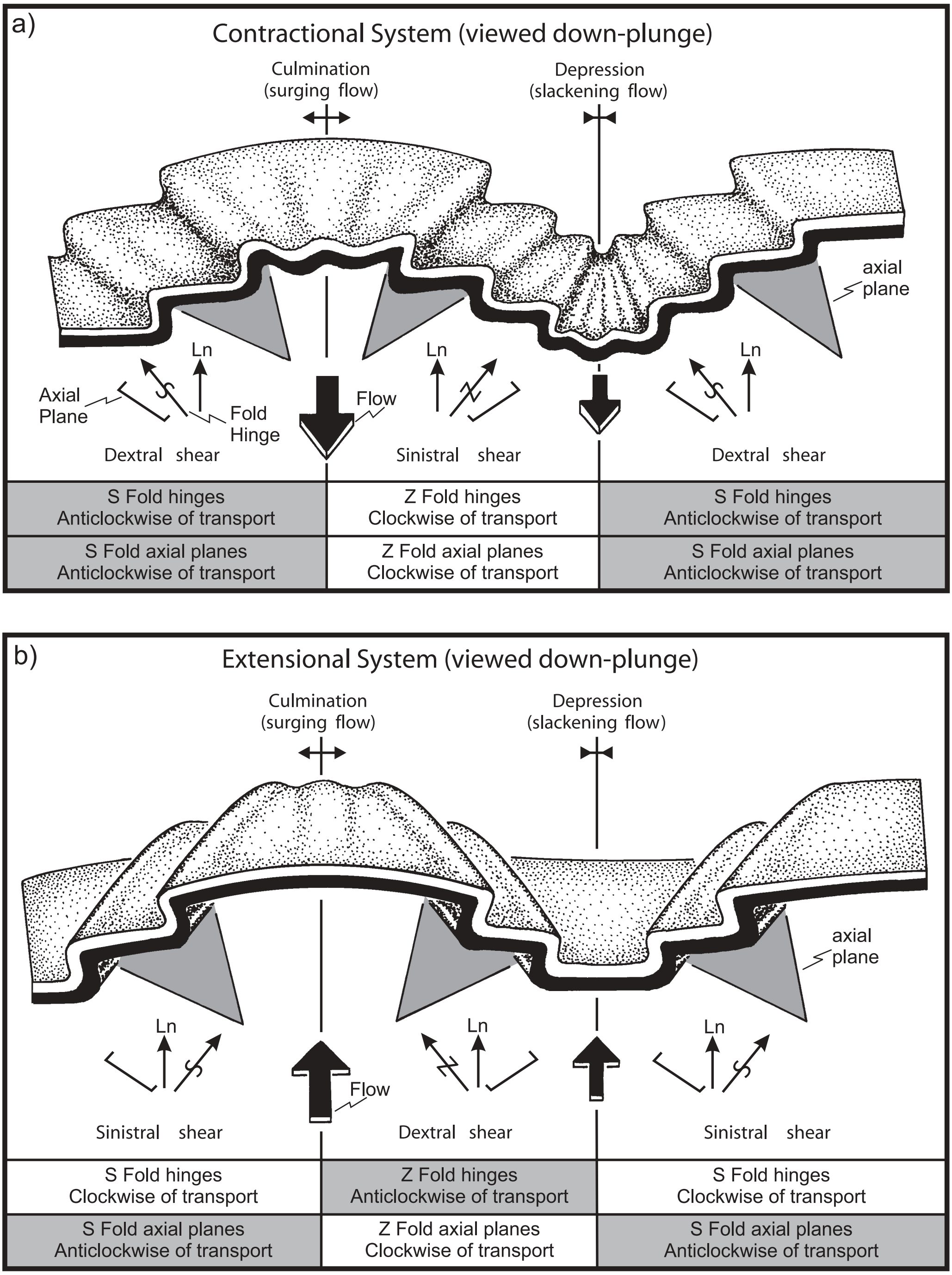

Fig. 12. In both contractional (**a**) and extensional (**b**) systems, the sense of axial planar obliquity remains constant with Z axial planes striking clockwise of transport, whereas S axial planes trend anticlockwise of transport (boxes with grey tone). The sense in which Z or S fold hinges pitch on their axial planes will, however, reverse (relative to L_n) from contractional to extensional systems. Flow directions (and relative velocities) are shown by the black arrows pointing towards the observer in the contractional system in (**a**) and away from the viewer in (**b**). (Refer to the text for further details.)

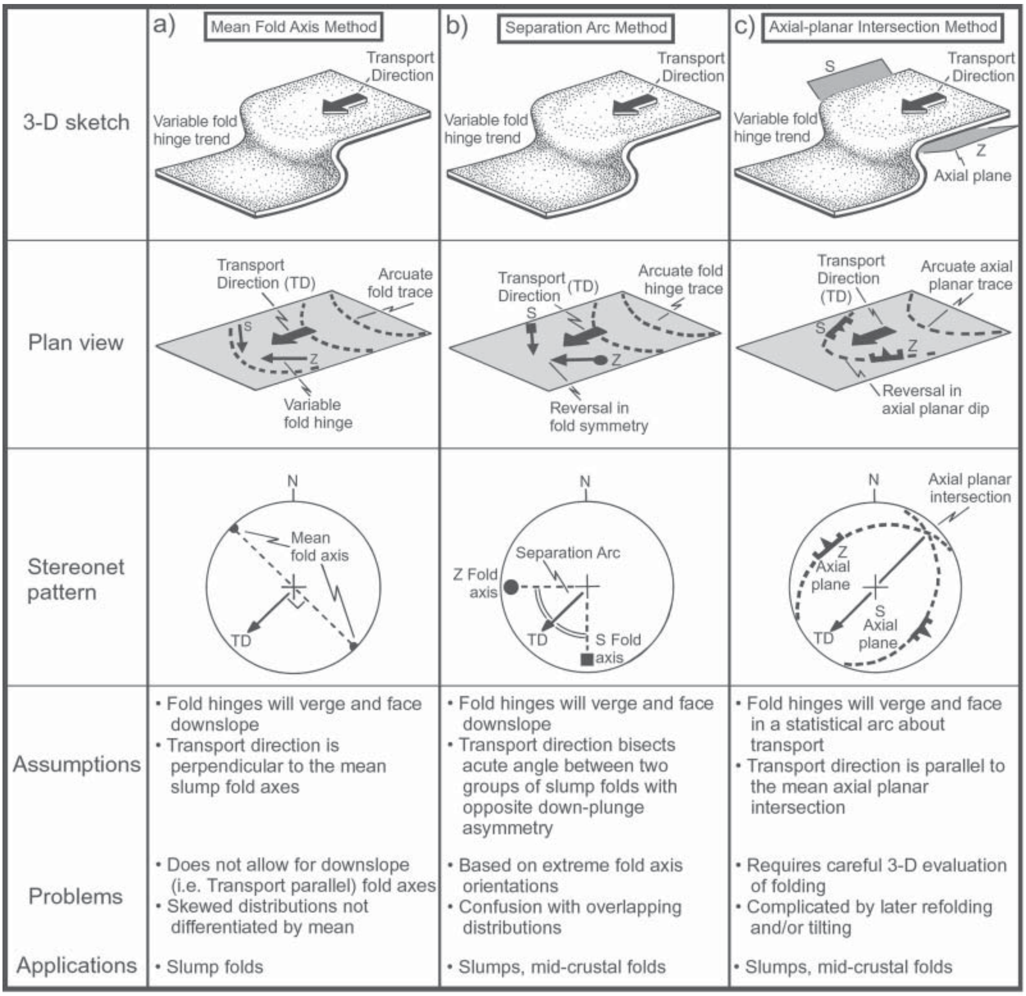

Fig. 13. Summary figure highlighting the principal methods for the determination of transport directions (TD) in a range of settings. The two existing principal techniques are the mean axis method (MAM) and the separation arc method (SAM). The axial-planar intersection method (AIM) utilizes the geometric fanning of mean Z and S fold axial planes about the flow direction to determine transport. (Refer to text for further details.)

the transport direction as the slump translates downslope. This will result in highly curvilinear sheath fold geometries in which the mean fold axis may be oblique (or even subparallel) to the flow direction, thereby resulting in highly inaccurate estimates of palaeoslope.

The separation arc method (SAM)

The second widely employed technique to determine the palaeoslope is the separation arc method (SAM) of Hansen (1965, 1967, 1971), who recognized that folds may display highly variable hinge orientations about the palaeoslope direction. This method assumes that the flow direction will bisect the acute angle between two groups of slump folds that display opposing down-plunge asymmetry (i.e. Z and S vergence; Fig. 13b). The problem with this approach, however, is the over-reliance on extreme fold hinge orientations to effectively constrain the bisecting transport direction. Further confusion may arise if the distribution of the two groups of asymmetric folds is overlapping thus negating any 'separation arc' with which to define the transport direction.

The axial-planar intersection method (AIM)

The dip of minor fold axial planes, associated with LNS-dominated flow perturbations, systematically increases as their strike becomes transport-parallel (Alsop & Holdsworth 2002, 2004*b*). This overall fanning arrangement also reflects S fold axial planes striking anticlockwise of transport, whereas Z fold axial planes strike clockwise. Typical flow patterns, incorporating both LPS and LNS components, will thus result in axial planes dipping in a listric arc about the transport direction. This relationship permits the trend and direction of tectonic transport to be reliably defined via the axial-planar intersection method (AIM). This technique involves simply calculating the mean axial planes of Z and S minor folds and then plotting these as great circles on a stereographic projection (Fig. 13c). The point of intersection of the mean Z and S great circles parallels the trend of tectonic transport. Within LPS-dominated settings, variably oriented minor folds, verging in the direction of transport, are marked by a listric arc of axial planes that dip into the flow direction. This sense of asymmetry thus provides the potential means of determining the direction of tectonic transport, which, in this (LPS) case, will form normal to the stereographic intersection of axial planes.

The AIM relies on mean axial-planar orientations for folds with opposing downslope vergence and is therefore statistically more robust than the SAM, which is dependent on extreme 'end-member' orientations to constrain transport. In addition, the AIM utilizes the inherent variability in hinge and axial-planar orientations that develop within a deforming mass undergoing differential shear at the margins. Consequently, it may be more reliable than the MAM, which will become highly inaccurate if folds are initiated during differential shear or are subjected to progressive deformation and rotation during translation.

Thus, the geometric arrangement of mean fold axial planes about the flow direction results in their intersection forming parallel to the transport direction. This relationship permits transport directions to be calculated via the AIM, and also allows comparison with the MAM and SAM, which were devised primarily for the study of soft-sediment deformation and palaeoslope analysis. This variability and fanning of minor fold axial planes allows the AIM to be used to determine transport directions in both contractional and extensional settings, and may also be applicable to a range of other environments in which material may flow and fold.

Conclusions

Flow perturbations are long-lived features capable of generating a range of primary sinuous fold patterns. Systematic analysis of such folds demonstrates that original fabric obliquities may be modified but not reversed during progressive deformation. As a consequence, they are extremely resilient to subsequent shearing and therefore may act as a reliable record of deformation. Fold hinge trends converge both along-strike, when crossing culmination or depression surfaces, and across-strike towards underlying higher strain detachments reflecting 3D variations in deformation within flow cells. Similar patterns are also shown by the strike of associated axial planes. The consistent senses of minor fold transection within flow perturbation folds reflect a component of progressive deformation and allow the sense of layer-normal differential shear to be determined. Such zones of layer-normal shear are also marked by patterns of reverse asymmetry vergence around the culmination, together with reversals in the polarity of structural facing, which is directed outwards from the culmination. In addition, the repeatability of the geometric relationships we have described allows these techniques to act as a reliable and predictive methodology in both contractional and extensional settings. In particular, the statistical fanning of minor fold axial planes within flow perturbations allows the transport direction to be determined by the axial-planar intersection method (AIM).

The (F_2) sheath folds and (F_3) synshearing flow folds in the Kyle of Tongue area share many geometric properties as both are related to the same top-to-the-WNW kinematic regime. Careful analysis of structural data on fabric topology plots demonstrates that curvilinear F_2 folding shows no distinct difference across the Kyle of Tongue marking the Ben Hope Thrust. However, F_3 folds are typically transport-subparallel to the east in the hanging wall of the Ben Hope Thrust and become transport-normal in its footwall. This pattern may be interpreted in terms of a switch from layer-normal shearing (LNS) in the hanging wall to layer-parallel shearing (LPS) in the footwall. The transport-parallel alignment of LPS and LNS culminations across the Ben Hope Thrust, together with the superposition of F_3 on F_2 culminations, indicates a component of structural inheritance on the location of successive perturbations, possibly with its origins in the underlying Lewisian basement rocks (Alsop *et al.* 1996).

The Ben Hope Thrust is folded and arched up by the transport-normal (LPS-dominated) F_3

folds in its footwall, whereas overlying transport-parallel (LNS-dominated) F_3 folds apparently root downwards onto it. These relationships are to be expected in a simple foreland-propagating system of ductile deformation. However, our analysis also shows that folds of similar 'F_3' generation may show variable relationships to underlying detachments both across- and along-strike. Thus, major transport-normal F_3 folds, west of the Kyle of Tongue, root into the underlying Achinver Thrust, which is itself folded farther north along-strike by transport-parallel F_3 folds in the Talmine area that root downwards into the Moine Thrust Zone mylonites. LNS appears to develop most readily in multilayer sequences such as the hanging wall of the Ben Hope Thrust and Talmine Imbricate Zone, whereas LPS typically forms in more homogeneous systems such as developed in psammites to the west of the Kyle of Tongue. Flow perturbation events therefore appear to be spatially recurrent features with long-lived control possible, related to material anisotropy. These relationships serve to highlight the complex interaction between flow cells associated with (1) broadly foreland-propagating deformation, (2) along-strike interplay between adjacent cells, and (3) homogeneous and heterogeneous multilayer sequences associated with LPS- and LNS-dominated flow, respectively.

Fieldwork for this paper was funded under the NERC–BGS Academic Mapping Programme awarded to the University of Durham (Grant F60/G2/36). Subsequent additional funding was provided from the Edinburgh Geological Society and the Irving and Welch bequests of the University of St. Andrews. The authors would especially like to thank R. Strachan and D. Cheer, together with the field trip participants of the 2002 shear zones meeting and the 2003 Highland workshop, for many interesting discussions concerning folding patterns in the Moine Nappe. Finally, we would like to thank H. Fossen and G. Lloyd for careful and constructive reviews of the manuscript.

References

Allen, M. B., Alsop, G. I. & Zhemchuzhnikov, V. G. 2001. Dome and basin refolding associated with transpressive inversion along the Karatau Fault System, southern Kazakstan. *Journal of the Geological Society, London*, **158**, 83–95.

Alsop, G. I. 1992. Progressive deformation and the rotation of contemporary fold axes in the Ballybofey Nappe, northwest Ireland. *Geological Journal*, **27**, 271–283.

Alsop, G. I. 1994. Relationships between distributed and localised shear in the tectonic evolution of a Caledonian fold and thrust zone, northwest Ireland. *Geological Magazine*, **131**, 123–136.

Alsop, G. I. & Holdsworth, R. E. 1993. The distribution, geometry and kinematic significance of Caledonian buckle folds in the western Moine Nappe, northwestern Scotland. *Geological Magazine*, **130**, 353–362.

Alsop, G. I. & Holdsworth, R. E. 1999. Vergence and facing patterns in large-scale sheath folds. *Journal of Structural Geology*, **21**, 1335–1349.

Alsop, G. I. & Holdsworth, R. E. 2002. The geometry and kinematics of flow perturbation folds. *Tectonophysics*, **350**, 99–125.

Alsop, G. I. & Holdsworth, R. E. 2004*a*. Shear zones — an introduction and overview. *In*: Alsop, G. I., Holdsworth, R. E., McCaffrey, K. J. W. & Hand, M. (eds) *Flow Processes in Faults and Shear Zones*. Geological Society, London, Special Publications, **224**, 1–9.

Alsop, G. I. & Holdsworth, R. E. 2004*b*. Shear zone folds: records of flow perturbation or structural inheritance? *In*: Alsop, G. I., Holdsworth, R. E., McCaffrey, K. J. W. & Hand, M. (eds) *Flow Processes in Faults and Shear Zones.* Geological Society, London, Special Publications, **224**, 177–199.

Alsop, G. I. & Holdsworth, R. E. 2004*c*. The geometry and topology of natural sheath folds: a new tool for structural analysis. *Journal of Structural Geology*, **26**, 1561–1589.

Alsop, G. I. & Holdsworth, R. E. 2005. Discussion on evidence for non-plane strain flattening along the Moine Thrust, Loch Strath nan Aisinnin, North-West Scotland by Strine & Wojtal. *Journal of Structural Geology*, **27**, 781–784.

Alsop, G. I. & Holdsworth, R. E. 2006. Sheath folds as discriminators of bulk strain type. *Journal of Structural Geology*, **28**, 1588–1606.

Alsop, G. I., Holdsworth, R. E. & Strachan, R. A. 1996. Transport-parallel cross folds within a mid-crustal Caledonian thrust stack, northern Scotland. *Journal of Structural Geology*, **18**, 783–790.

Bell, T. H. 1978. Progressive deformation and reorientation of fold axes in a ductile mylonite zone: the Woodroffe thrust. *Tectonophysics*, **44**, 285–321.

Berthé, D. & Brun, J. P. 1980. Evolution of folds during progressive shear in the South Amorican Shear Zone, France. *Journal of Structural Geology*, **2**, 127–133.

British Geological Survey 1997. *Tongue, Scotland 114E.* Solid Geology, 1:50 000.

British Geological Survey 2002. *Loch Eriboll, Scotland 114W.* Solid Geology, 1:50 000.

Bryant, B. & Reed, J. C. 1969. Significance of lineation and minor folds near major thrust faults in the southern Appalachians and the British and Norwegian Caledonides. *Geological Magazine*, **106**, 412–429.

Carreras, J., Estrada, A. & White, S. 1977. The effect of folding on the *c*-axis fabrics of a quartz mylonite. *Tectonophysics*, **39**, 3–24.

Cobbold, P. R. & Quinquis, H. 1980. Development of sheath folds in shear regimes. *Journal of Structural Geology*, **2**, 119–126.

Coward, M. P. 1982. Surge zones in the Moine thrust zone of NW Scotland. *Journal of Structural Geology*, **4**, 247–256.

Coward, M. P. 1983. The thrust and shear zones of the Moine thrust zone and the NW Scottish Caledonides. *Journal of the Geological Society, London*, **140**, 795–811.

Coward, M. P. 1984. The strain and textural history of thin-skinned tectonic zones: examples from the Assynt region of the Moine Thrust zone, NW Scotland. *Journal of Structural Geology*, **6**, 89–99.

Coward, M. P. & Kim, J. H. 1981. Strain within thrust sheets. *In*: McClay, K. R. & Price, N. J. (eds) *Thrust and Nappe Tectonics.* Geological Society, London, Special Publications, **9**, 275–292.

Coward, M. P. & Potts, G. J. 1983. Complex strain patterns developed at the frontal and lateral tips to shear zones and thrust zones. *Journal of Structural Geology*, **5**, 383–399.

Downing, K. N. & Coward, M. P. 1981. The Okahandja Lineament and its significance for Damaran tectonics in Namibia. *Geologische Rundshau*, **70**, 972–1000.

Dubey, A. K. & Cobbold, P. R. 1977. Noncylindrical flexural slip folds in nature and experiment. *Tectonophysics*, **38**, 223–239.

Elliot, D. 1976. The energy balance and deformation mechanisms of thrust sheets. *Philosophical Transactions of the Royal Society of London*, **283**, 289–312.

Escher, A. & Watterson, J. 1974. Stretching fabrics, folds and crustal shortening. *Tectonophysics*, **22**, 223–231.

Evans, D. J. & White, S. H. 1984. Microstructural and fabric studies from the rocks of the Moine Nappe, Eriboll, NW Scotland. *Journal of Structural Geology*, **6**, 369–389.

Farrell, S. G. 1984. A dislocation model applied to slump structures, Ainsa Basin, South Central Pyrenees. *Journal of Structural Geology*, **6**, 727–736.

Fink, J. 1980. Surface folding and viscosity of rhyolite flows. *Geology*, **8**, 250–254.

Fossen, H. & Rykkelid, E. 1990. Shear zone structures in the Øygarden area, West Norway. *Tectonophysics*, **174**, 385–397.

Ghosh, S. K. & Ramberg, H. 1968. Buckling experiments on intersecting fold patterns. *Tectonophysics*, **5**, 89–105.

Ghosh, S. K. & Sengupta, S. 1984. Successive development of plane noncylindrical folds in progressive deformation. *Journal of Structural Geology*, **6**, 703–709.

Ghosh, S. K. & Sengupta, S. 1987. Progressive development of structures in a ductile shear zone. *Journal of Structural Geology*, **9**, 277–287.

Goscombe, B. 1991. Intense non-coaxial shear and the development of mega-scale sheath folds in the Arunta Block, Central Australia. *Journal of Structural Geology*, **13**, 299–318.

Hambrey, M. J. & Lawson, W. 2000. Structural styles and deformation fields in glaciers: a review. *In*: Maltman, A. J., Hubbard, B. & Hambrey, M. J. (eds) *Deformation of Glacial Materials.* Geological Society, London, Special Publications, **176**, 59–83.

Hansen, E. 1965. Methods of deducing slip-line orientations from the geometry of folds. *Carnegie Institution of Washington Yearbook*, **65**, 387–405.

Hansen, E. 1967. Natural slip folds in which the fold axes nearly parallel the slip lines. *Carnegie Institution of Washington Yearbook*, **66**, 536–538.

Hansen, E. 1971. *Strain Facies.* Springer, New York.

Holdsworth, R. E. 1988. The stereographic analysis of facing. *Journal of Structural Geology*, **10**, 219–223.

Holdsworth, R. E. 1989. The geology and structural evolution of a Caledonian fold and ductile thrust zone, Kyle of Tongue region, Sutherland, N. Scotland. *Journal of the Geological Society, London*, **146**, 809–823.

Holdsworth, R. E. 1990. Progressive deformation structures associated with ductile thrusts in the Moine Nappe, Sutherland, N. Scotland. *Journal of Structural Geology*, **12**, 443–452.

Holdsworth, R. E. & Grant, C. J. 1990. Convergence-related 'dynamic spreading' in a mid-crustal ductile thrust zone: a possible orogenic wedge model. *In*: Knipe, R. J. & Rutter, E. H. (eds) *Deformation Mechanisms, Rheology and Tectonics.* Geological Society, London, Special Publications, **54**, 491–500.

Holdsworth, R. E. & Roberts, A. M. 1984. A study of early curvilinear fold structures and strain in the Moine of the Glen Garry region, Inverness-shire. *Journal of the Geological Society, London*, **141**, 327–338.

Holdsworth, R. E., Strachan, R. A. & Alsop, G. I. 2001. *Geology of the Tongue District.* Memoirs of the British Geological Survey, Sheet 114E (Scotland).

Holdsworth, R. E., Alsop, G. I. & Strachan, R. A. 2007. Tectonic stratigraphy and structural continuity of the northernmost Moine Thrust Zone and Moine Nappe, Scottish Caledonides. *In*: Ries, A. C., Butler, R. W. H. & Graham, R. H. (eds) *Deformation of the Continental Crust: The Legacy of Mike Coward.* Geological Society, London, Special Publications, **272**, 121–142.

Jones, O. T. 1940. The geology of the Colwyn Bay district: study of submarine slumping during the Salopian Period. *Quarterly Journal of the Geological Society of London*, **95**, 335–382.

Lacassin, R. & Mattauer, M. 1985. Kilometre-scale sheath fold at Mattmark and implications for transport directions in the Alps. *Nature*, **315**, 739–742.

Lajoie, J. 1972. Slump fold axis orientations: an indication of paleoslope? *Journal of Sedimentary Petrology*, **42**, 584–586.

Lawson, W. J., Sharp, M. J. & Hambray, M. J. 1994. The structural geology of a surge-type glacier. *Journal of Structural Geology*, **16**, 1447–1462.

McClay, K. R. 1987. *The Mapping of Geological Structures*. Geological Society, London, Handbook.

Mies, J. W. 1991. Planar dispersion of folds in ductile shear zones and kinematic interpretation of fold hinge girdles. *Journal of Structural Geology*, **13**, 281–297.

Minnigh, L. D. 1979. Structural analysis of sheath-folds in a meta-chert from the Western Italian Alps. *Journal of Structural Geology*, **1**, 275–282.

PLATT, J. P. 1983. Progressive refolding in ductile shear zones. *Journal of Structural Geology*, **5**, 619–622.

QUINQUIS, H., AUDREN, C., BRUN, J. P. & COBBOLD, P. R. 1978. Intense progressive shear in Ile de Groix blueschists and compatibility with subduction or obduction. *Nature*, **273**, 43–45.

RAMSAY, J. G. 1980. Shear zone geometry: a review. *Journal of Structural Geology*, **2**, 83–99.

RAMSAY, J. G. & LISLE, R. 2000. *The Techniques of Modern Structural Geology. Volume 3: Applications of continuum Mechanics in Structural Geology*. Academic Press, London.

RHODES, S. & GAYER, R. A. 1977. Non-cylindrical folds, linear structures in the X-direction and mylonite developed during translation of the Caledonian Kalak Nappe Complex of Finnmark. *Geological Magazine*, **114**, 329–341.

RIDLEY, J. 1986. Parallel stretching lineations and fold axes oblique to displacement direction — a model and observations. *Journal of Structural Geology*, **8**, 647–654.

ROBERTS, A. 1989. Fold and thrust structures in the Kintradwell 'Boulder beds', Moray Firth. *Scottish Journal of Geology*, **25**, 173–186.

SANDERSON, D. J. 1973. The development of fold axes oblique to the regional trend. *Tectonophysics*, **16**, 55–70.

SHACKLETON, R. M. 1958. Downward-facing structures of the Highland Border. *Quarterly Journal of the Geological Society of London*, **113**, 361–392.

SKJERNAA, L. 1980. Rotation and deformation of randomly oriented planar and linear structures in progressive simple shear. *Journal of Structural Geology*, **2**, 101–109.

SKJERNAA, L. 1989. Tubular folds and sheath folds: definitions and conceptual models for their development with examples from the Grapesvare area, northern Sweden. *Journal of Structural Geology*, **11**, 689–703.

STRACHAN, L. J. 2002. Slump-initiated and controlled syndepositional sandstone remobilization: an example from the Namurian of County Clare, Ireland. *Sedimentology*, **49**, 25–41.

STRACHAN, R. A., SMITH, M., HARRIS, A. L. & FETTES, D. J. 2002. The Northern Highland and Grampian Terranes. *In*: TREWIN, N. (ed.) *Geology of Scotland.* Geological Society, London, 81–147.

STRACHAN, L. J. & ALSOP, G. I. 2006. Slump folds as estimators of palaeoslope: a case study from the Fisherstreet slump of County Clare, Ireland. *Basin Research*, **18**, 451–470.

TALBOT, C. J. 1979. Fold trains in a glacier of salt in southern Iran. *Journal of Structural Geology*, **1**, 5–18.

TALBOT, C. J. & AFTABI, P. 2004. Geology and models of salt extrusion at Qum Kuh, central Iran. *Journal of the Geological Society, London*, **161**, 321–334.

TALBOT, C. J. & JARVIS, R. J. 1984. Age, budget and dynamics of an active salt extrusion in Iran. *Journal of Structural Geology*, **6**, 521–533.

WATKINSON, A. J. & COBBOLD, P. R. 1981. Axial directions of folds in rocks with linear/planar fabrics. *Journal of Structural Geology*, **3**, 211–217.

WILLIAMS, G. D. 1978. Rotation of contemporary folds into the X direction during overthrust processes in Laksefjord, Finnmark. *Tectonophysics*, **48**, 29–40.

WOODCOCK, N. H. 1979. The use of slump structures as palaeoslope orientation estimators. *Sedimentology*, **26**, 83–99.